KONA Powder and Particle Journal

KONA Powder and Particle Journal No. 42 (2025) 170–187/https://doi.org/10.14356/kona.2025004 Review Paper

Review of the Gas-Phase Synthesis of Particle Heteroaggregates and Their Applications †

Suman Pokhrel [1,2,3], Udo Fritsching [1,2,3] and Lutz Mädler [1,2,3]*

[1] *Particles and Process Engineering, Faculty of Production Engineering, University of Bremen, Germany*
[2] *Leibniz Institute for Materials Engineering, Germany*
[3] *MAPEX Center for Materials and Processes, University of Bremen, Germany*

Custom-made nanomaterials are indispensable in the production of high-value goods in almost any industry. For many applications, materials with defined functional contacts on the nanoscale between different components are crucial. In heterogeneous catalysis, active nanoparticles are often dispersed on a support, and defined interfaces facilitate the stabilization of the active materials. This leads to strong metal-support interactions (SMSI), which determine the activity and selectivity of the catalytic reactions. In photocatalysts, hetero-contacts can significantly reduce electron–hole recombination after light excitation, leading to improved photoefficiency. By choosing materials with appropriate band levels, the redox window can be tuned for a specific reaction. In batteries, mixing the active material and carbon leads to improved electrochemical characteristics. All these applications have in common that different nanomaterials need to be mixed at the nano-level with defined interfaces. This review highlights the most suitable routes for gas-phase synthesis of particle heteroaggregates, their modeling, and their applications.

Keywords: double flame spray pyrolysis, aerosol mixing, heteroaggregates, heterojunctions, charge transfer

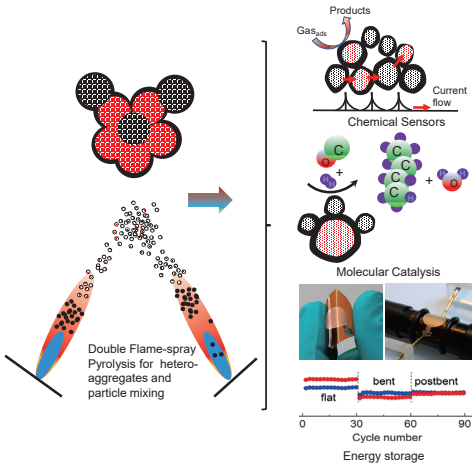

1. Introduction

Various synthesis techniques are possible to produce highly defined particle mixtures at the nanoscale (Minnermann et al., 2011; 2013). These can be broadly distinguished in processes where readily produced nanoparticles are mixed in the liquid phase (Grossmann, 2017; Grossmann et al., 2015; Shi and Russell, 2018). To mix these two dissimilar nanoparticles in the liquid, the break-up of agglomerated and even aggregated nanoparticles needs to be achieved, e.g., by milling, dispersion in a sonic nozzle, or ultrasonification of nanoparticles in liquid (Wang et al., 2015). In the second step, a heat treatment process leads to the formation of interfaces in a single step during solid-state particle synthesis (Yu et al., 2021). In well-known wet-chemical approaches, such as sol–gel, precipitation, or incipient wetness techniques, the formation of an interface is achieved by modifying the temperature, pressure, solvent composition (Munnik et al., 2015). A major drawback of wet-chemical approaches is achieving good crystallinity and the requirement of additional calcination/heat treatment steps for the modification of the material interface (Sun et al., 2015; 2016). Gas-phase preparation, especially coupled with high-temperature synthesis of nanoparticles, offers a scalable, single-step alternative to established wet-chemical synthesis routes (Lovell et al., 2019; Pokhrel et al., 2013). A promising technique for designing such heterointerfaces is the double flame spray pyrolysis (DFSP) approach (Gäßler et al., 2022; Stahl et al., 2021). Here, nanoparticle components are synthesized in two individual flame sprays that are mixed at a certain distance above the burners (Kim et al., 2016; Wang et al., 2013). Parameters such as nozzle distances, air entrainment rate, turbulence of the mixing jets, and temperature distribution are important for controlling the mixing process (Minnermann et al., 2011; 2013). High-temperature gradients in the process from ~2800 °C in the flames to almost room temperature in just a few milliseconds and lateral scales of millimeter lead to highly crystalline primary particles (Balakrishnan et al., 2021; Li et al., 2020; Pokhrel et al., 2023). Gas-phase synthesis of multicomponent nanomaterials has huge potential, but a review of different gas-phase mixing approaches is still lacking.

In this contribution, we discuss the routes and process parameters for determining aggregation in gas-phase

† Received 4 July 2023; Accepted 5 September 2023
J-STAGE Advance published online 24 February 2024
* Corresponding author: Lutz Mädler;
[1,3] Add: Badgasteiner Straße 1, 28359 Bremen, Germany
[2] Add: Badgasteiner Straße 3, 28359 Bremen, Germany
E-mail: lmaedler@iwt.uni-bremen.de
TEL: +49-421-21851200

mixing processes. Here, computational fluid dynamics (CFD) simulations coupled with discrete element methods (DEM) or population balance methods (PBM) that can simulate interface formation between nanoparticles in the gas phase are discussed. Techniques for experimentally determining the mixing state of multiple particles are introduced. Currently, different communities studying gas-phase mixing of nanomaterials often use different definitions, leading to possible misunderstandings. Thus, the review will recommend some unification and common definitions for core concepts such as interfaces, heteroaggregates, (functional) hetero-contacts/junctions, and even aggregation. Applications of heteroaggregates designed using double flame spray pyrolysis are discussed, validating that gas-phase mixing research serves as a common reference point for the future. Heterojunctions in aggregates are created by physically mixing dissimilar particles such as A and B or directly nucleating one dissimilar particle on the other during the synthesis process. The number density of the hetero-contacts and their distribution determine the reaction kinetics, adsorption sites, and reaction centers (Lovell et al., 2019). In addition to the chemical composition of the particles, the shape and surface morphology of the heteroaggregates are key to the overall material performance.

2. Gas-phase in situ mixing to design heteroaggregates

An aggregate confines multiple, and chemically tight, sintered primary particle—a characteristic property of gas-phase synthesized materials (Eggersdorfer et al., 2012). The degree of mixing indicates the number density of hetero-contacts between different dissimilar particles and is abundant when all particles are bonded via hetero-contacts. The high thermal gradient due to radiation, evaporation, and collision of the saturated aerosol stream (particle clusters/nuclei) allows efficient particle mixing. Feng et al. (2015; 2016) described continuous gas-phase synthesis using lasers or electric discharge to produce vapor through material ablation. The vapor was quenched using an inert gas co-flow. While supersaturation is realized in such quenched vapor, the critical nucleus size is reduced to the atomic scale, causing strong coagulation and particle growth. A key paradigm is singlets, i.e., single particles grow from clusters to sizes up to a few nanometers, forming primary particles in aggregates. In another report, Voloshko et al. (2015) studied the particle formation process in spark discharge and nanosecond- (ns-)laser ablation, focusing on the plasma influence on particle formation. In both techniques, Cu was used as the target material. Although the plasma density and time evolution were different, the particles were similar because of the larger evaporation rate in ns-laser ablation and supersaturated vapor formation in the spark. In the spark discharge process, nanoparticles are generated by evaporation followed by condensation. First, the spark enables the evaporation of the target material, followed by subsequent rapid quenching via adiabatic expansion of the plasma radiation, and mixes with the carrier gas to result in supersaturation of the vapor. As stated earlier, higher saturation triggers nucleus formation, coagulation, and particle growth. Tabrizi et al. (2009) postulated that the co-evaporation of different materials from the target electrodes leads to the formation of mixed particles. Based on this hypothesis, Pfeiffer et al. (2014) investigated the formation of Pd-doped Mg heteroaggregates using a double spark mixing process. The vapor generated from each individual spark was rapidly cooled via adiabatic expansion and instantly mixed with one another using co-flow gas. While a very high-temperature gradient and vapor supersaturation are achieved in the spark-generated vapor, the Smoluchowski-type coagulation process dominates. This process allows simultaneous evaporation of different materials, which combine to form new heteroaggregates. Hence, gas-phase aerosol mixing is very attractive for heteroaggregate systems where a wide range of precursors with low volatility and high energy combustion density are available (Marine et al., 2000). In addition, homogeneity of the particle–particle mixture is realized when the hetero-contacts are uniformly distributed from the surface to the bulk of the particle ensemble. Note that two or more multicomponent mixtures at the atomic scale lead either to the formation of a mixed metal oxide or to a doped system (Adeleye et al., 2018; Naatz et al., 2017). Such a system represents an individual particle (classified as binary, ternary and quaternary) with a crystal structure of at least two different elements having a covalent bond with the ligand. The ternary forms include perovskites (ABO_3), scheelites (ABO_4), spinels (AB_2O_4), and even ternary metastable phases that are used in a variety of catalytic systems (Dreyer et al., 2016; Grossmann, 2017; Kemmler et al., 2012). As an example, these heteroaggregates are obtained in the gas phase by double flame spray pyrolysis (DFSP), which can synthesize a variety of heteroaggregates.

Two aerosol streams (containing independent components) from two separate spray flames at different temperatures and at different stages of particle formation within the individual aerosol stream can be mixed (**Fig. 1**). The materials nucleate in different flames, and the intersection of the two flames at a defined distance and angle results in a certain mixing state. The geometric configuration and the corresponding process conditions (e.g. temperature) in the mixing zone significantly influence the material properties. The concentration ratio of the sprayed components and the adjustment of the flame geometry allow tailored synthesis of mixing states within a single and/or agglomerated particle. A single-step synthesis of these different mixing stages is achieved when DFSP is applied. The particle residence

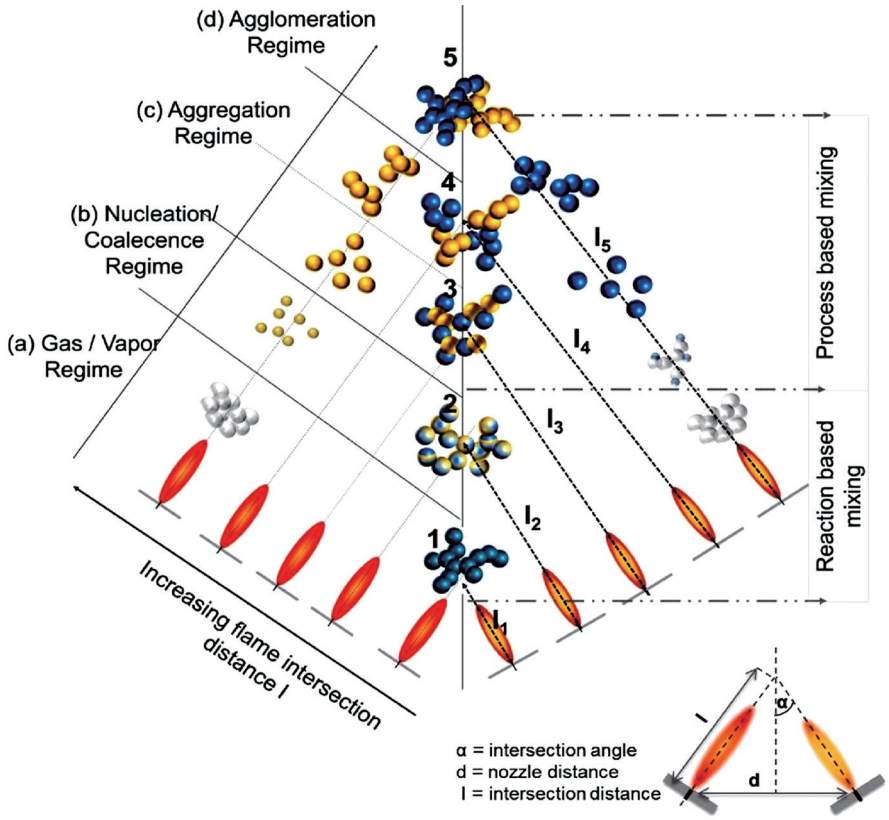

Fig. 1 Illustration of the influence of the intersection distance and mixing within the aggregated systems. **(a)** The intersection distance of the flames when both precursors are in the gas/vapor phase results in atomic mixing to form heteroaggregates. **(b)** Mixing in a zone, where nucleation and primary particle formation start, can result in the formation of polycrystalline particles. The characteristics of the synthesized particles highly depend on the miscibility of the material. High miscibility favors polycrystalline particle formation due to diffusion processes. **(c)** An increase in the flame intersection distance up to the aggregation regime favors the formation of individual oxide particles, which form a mixture on the particle scale. **(d)** A further increase in the intersection distance, associated with a decrease in the temperature in the mixing zone, leads to a mixture on the agglomerate scale. The aggregates physically bond to one another. Adapted from Grossmann (2017). Copyright Universität Bremen Library, open access (URN: urn:nbn:de:gbv:46-00106641-10).

times of the two streams through symmetrical and/or non-symmetrical mixing can be exploited to vary the particle properties. External temperature control at the mixing point is possible by installing a quenching ring at the point of aerosol mixing. The high thermal gradient of individual aerosol streams enables independent control of the specific surface area of the particles and their crystallinity (Kemmler et al., 2012). The hetero-contact of different binary, ternary, mixed binary, and mixed ternary materials obtained in the gas phase is crucial for particle performance. The in situ synthesis of the materials using different flame symmetries and nozzle placements enabled the formation of such heteroaggregates. Integrated high-temperature aerosol synthesis with multiple flames is a promising route for complex and heteroaggregated materials via various precursor/solvent combinations, concentrations, temperature profiles, and residence times in the flame (Buss et al., 2019; Meierhofer and Fritsching, 2021; Meierhofer et al., 2017; Pokhrel et al., 2010; Pokhrel and Mädler, 2020). Each flame producing the desired oxide mixtures and/or single metastable phases is characterized by its own temperature profile along the axis of the gas flow. This results in a specific temperature–time history during nanoparticle formation. It is known that increasing the precursor flow rate and decreasing the dispersion gas lead to a longer flame and residence time, resulting in the production of larger particles. The gas composition (air or oxygen) and the energy provided by the supporting flame are further measures to tune the temperature–time history. In the direct mixing of existing particle systems, particle concentration plays a key role. The particle formation process using large nozzle distances allows the physical mixing of the two heteroaggregates at the mixing zone. Aerosol mixing within the nucleation phase leads to atomic mixing producing ternary and/or metastable phases. However, when the mixing process occurs later, i.e., when the two aerosol streams mix at a higher distance above the nozzle, heteroaggregates are obtained. If the respective aerosol streams are mixed even later, the particles and agglomerates produce fewer hetero-contacts. Based on this strategy, Co/Al_2O_3 Fischer–Tropsch catalysts were synthesized using Co and Al aerosol streams (Schubert et al., 2016). When these two streams

were mixed before the nucleation phase, a very stable but catalytically inactive mixed phase ($Co_{3-x}Al_xO_4$, $0 < x \leq 2$) was formed. However, mixing the two aerosol streams after the nucleation phase gives rise to homogeneously mixed heteroaggregates, allowing a very active Co catalyst in stable Al_2O_3 support. Hetero-contact plays an essential role, especially in the dry reforming of CH_4, which was demonstrated by the selective mixing of even three-component systems (Horlyck et al., 2019). Note that the mismatch of the primary particle size induces random collisions during aerosol mixing between two dissimilar particles, resulting in heteroaggregates. The formation of larger particles could be counteracted by reducing the precursor concentration and increasing the oxidant flow. Recently, the degree of mixing as a function of time was acquired via DEM simulation in a rotary drum. This new strategy is based on cross-correlation development from a learning set consisting of 17 sets of simulation data representing a variation in the revolution frequency. The results showed good predictions for binary mixtures of particles with different densities rather than sizes within the parametric conditions (Wu et al., 2022). Therefore, double flame FSP is a versatile technique in which each precursor component is subjected to the same temperature–time history, leading to atomically mixed metal oxide NPs. However, the quantification of hetero-contacts generated from such gas-phase synthesis is challenging and requires extensive theoretical and mathematical models to clarify. In addition, the type of hetero-contact (physical and/or chemical with respect to a contact energy) and the possibilities for flexible adjustment allow the extraction of material properties.

3. Modeling and theoretical characterization of heteroaggregation

The modeling approaches of aerosol particle formation are based on gas-to-particle growth mechanisms depicted in **Figs. 2(a) and (b)**, where the time scales of chemical reactions are much shorter than the particle residence time in the reactor (Pratsinis, 1998). Although DEM for the analysis of particle processes is already developed (Pöschel and Schwager, 2005) and used for the description of large particle systems (Fischer et al., 2016; Parteli and Pöschel, 2016), the modeling of aerosol reactors for the description of homogenization and aggregation processes on the sub-micron scale appears to be a challenge. This concerns the inclusion of short-range surfaces (e.g., van der Waals) and electrostatic forces, which are dominant for these particle sizes and heteroaggregates (Endres et al., 2021; Parteli et al., 2014). Very recently, Endres et al. (2021) reported particle–particle interactions in flame-made agglomerates. Such interactions were described using a particle–particle contact model assuming inherent material properties such as but not limited to mechanical stiffness, plasticity, polarizability, surface charge, and chemistry (Endres et al., 2021; Parteli et al., 2014). Numerical modeling of such particles and aggregates of very different sizes and complex geometric shapes requires the development of new approaches in DEM and much more elaborate algorithmic description for high-performance computing (HPC) (Endres et al., 2022; Gunkelmann et al., 2014; Topic and Pöschel, 2016).

In a very early work on combustion, Ulrich and Subramanian (1977) reported a model for coagulation and sintering mechanisms as growth-limiting and process-controlling mechanisms. Later, Kruis et al. (1993) modified the model by considering a characteristic sintering time and introducing a fractal dimensional parameter to describe the particle aggregates. Johannessen et al. (2000) reported a mathematical model for the dynamics of particle growth during the synthesis of ultrafine particles in diffusion flames. The velocity, temperature, and gas composition in a diffusion flame for Al_2O_3 synthesis were calculated by

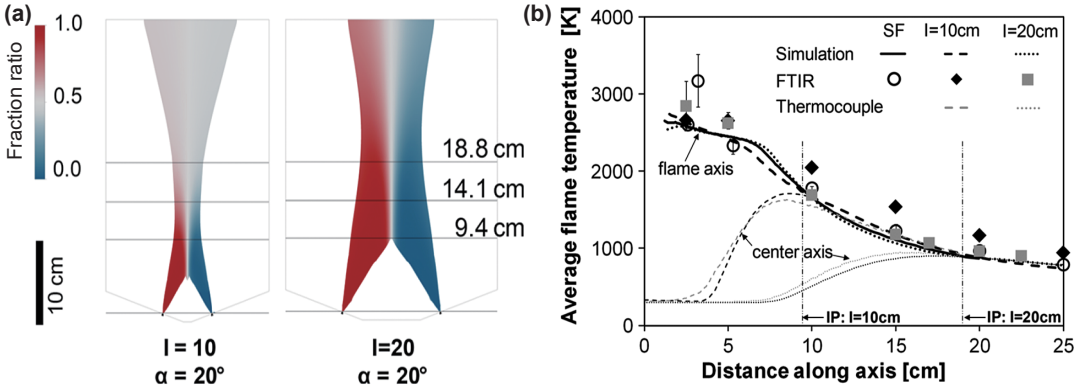

Fig. 2 Numerical simulations of two-particle aerosol mixing (from double flame spray pyrolysis) reported by Grossmann et al. **(a)** Central plane contour plots of the fraction ratio released from nozzles 1 (red) and 2 (blue) for the $l = 10$ cm and $l = 20$ cm settings are inclined at 20°. **(b)** FTIR-measured line-of-sight (symbols) and CFD-predicted centerline flame temperatures (thick black lines) along the flame axis for the single flame (circles, solid line) as well as the DF with $l = 10$ cm (diamonds, dashed line) and $l = 20$ cm (squares, dotted line) inclined at 20°. The specific influence of the process flow and the process conditions are decisive for the resulting heteroaggregates and their properties. Adapted from Grossmann et al. (2015). Copyright 2015, Springer.

simplification of 2D simulations of the aerosol model. The model was a key to developing an aerosol solver that allows detailed representation of particle evolution within the calculated process domain (Gröhn et al., 2011). To control the particle growth and mixing processes of heteroaggregation, complex simulation models for different aerosol flame reactor configurations have been analyzed (Meierhofer et al., 2014; Noriler et al., 2014). Meierhofer et al. (2014) reported numerical simulations of the air entrainment and droplet trajectory of the flame spray. At very low swirl angles (0°), droplets explicitly splashed on the nozzle plate. A similar calculation at 5° showed that the recirculation of the particles forced the small droplets toward the flame. The increase in the swirl angle to 15° directed all the droplets toward the flame with completely reduced recirculation. The simulation data showed that the stronger swirling flow prolonged the mean residence time of the droplets in the combustion domain for aggregate formation (Mädler et al., 2002; Meierhofer et al., 2014). Grossmann et al. (2015) reported a mathematical model describing the reactive spray dynamics of xylene using a two-phase Euler–Lagrange approach describing the continuous gas phase and discrete liquid droplets. The simulation for the temperature is underestimated, whereas the FTIR data shows the average temperature in regions with steep radial gradients. Lowering the intersection distances of the two aerosol streams increases the temperature up to 300 K along the flame axis between 10 and 20 cm [**Figs. 2(a) and (b)**]. Hence, the fundamental understanding of gas-phase particle production is through simulation and modeling of the process, enabling tailor-made functional particles with an enhanced number of hetero-contacts.

While reactor geometry and process parameter models are important for understanding particle production, theoretical characterization of nanosized heteroaggregates requires mixing characteristics during such processes. Baric et al. (2018) studied the mixing properties of flame-made particles using a combination of particle simulations and image analysis to derive correlations for the quantification of particle mixing. The acquired simulation method predicted the 3D coordination number from 2D images of binary and/or ternary mixtures of aggregated particles. This method is valid for cluster aggregation with primary particles >4. The results of binary particle mixing (between the simulations and experimental imaging) showed that the coordination numbers and cluster sizes deviate from the simulated values by ~10 % (mixing ratio 0.6 and 0.7) and below 30 % (mixing ratio 0.8), respectively.

Very recently, Gerken et al. (2023) validated the work reported by Baric et al. They used double flame-sprayed TiO_2 and WO_3 heteroaggregates to quantify hetero-contacts using high-angle annular dark-field scanning transmission electron microscopy (HAADF-STEM) images. The heteroaggregates shown in **Fig. 3** were generated as 3D objects in the computer. The figure is a corresponding 2D projection of the 3D aggregates from the simulation. In contrast to the 2D image analysis in the experiment, it is possible to simulate 3D particle systems and subsequently convert them into a 2D projection to mimic the image analysis by TEM. This allows a direct correlation between 2D and 3D cluster sizes and coordination numbers (Baric et al., 2018). The approach based on a geometric model considered the ratio of sample thickness and logarithmically scaled colored intensity. The data showed that in all the cases, each primary nanoparticle had ~10 % of another particles (either WO_3 during TiO_2 quantification or vice versa) during EDX measurements. The tool developed was reported as generic, which could be used for any such

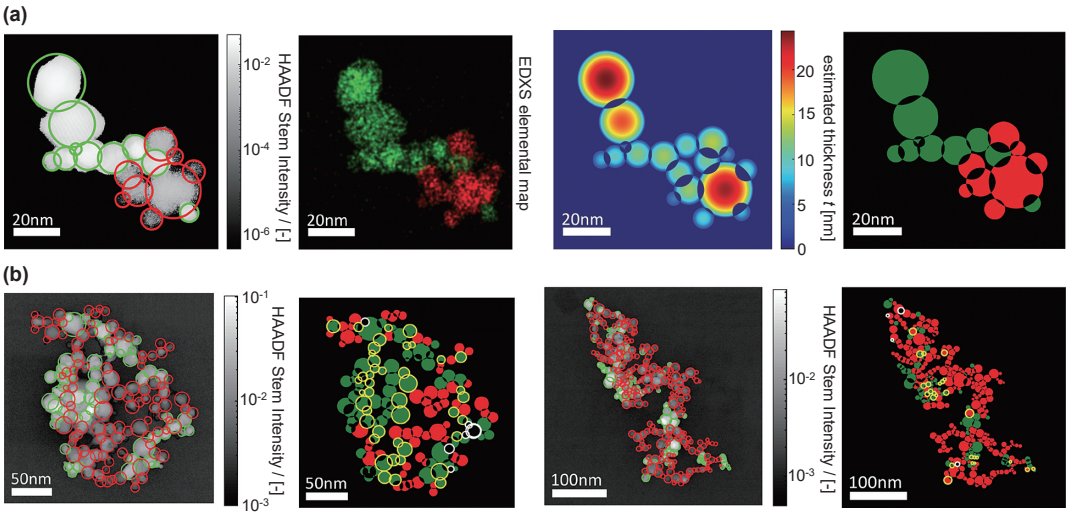

Fig. 3 HAADF STEM image of an exemplary TiO_2–WO_3 heteroaggregate. From left to right, the particle (TiO_2/WO_3) positions are marked manually; the red circle represents TiO_2 while the green circle represents WO_3. The elemental map was scanned using EDXS and the particle thickness was estimated by a geometric model assuming spherical particles **(a)** for small heteroaggregates and **(b)** large heteroaggregates. Adapted from Gerken et al. (2023). Copyright 2023 Wiley.

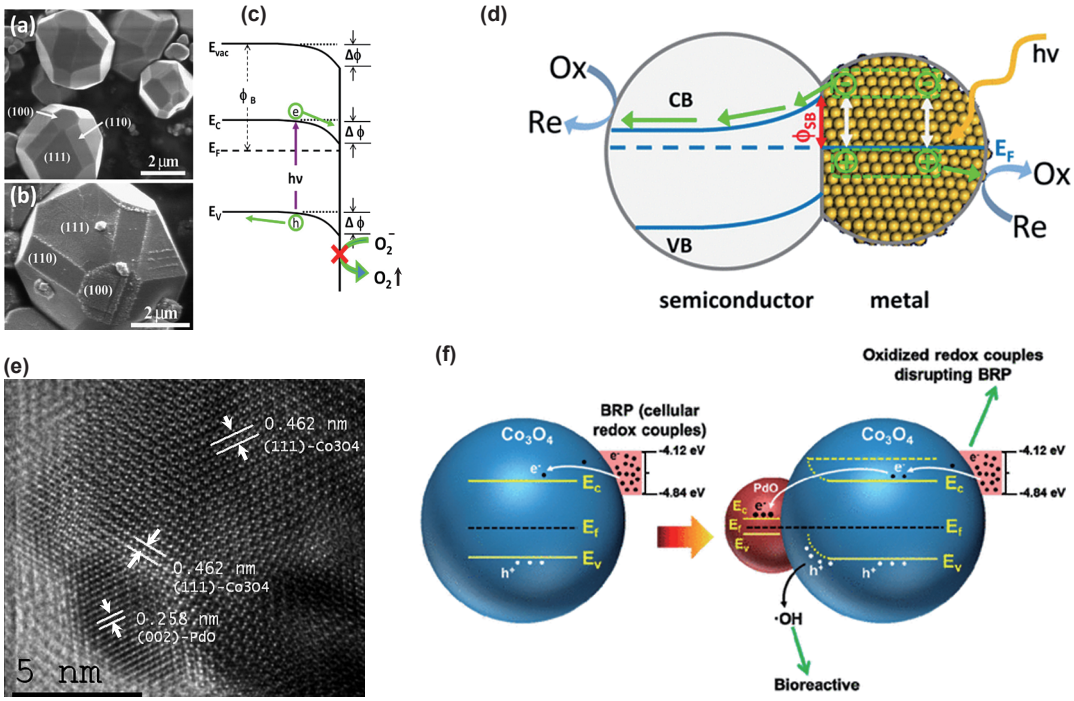

Fig. 4 SEM images of highly crystalline $BaTiO_3$ produced in **(a)** KCl and **(b)** after reaction in aqueous $AgNO_3$. Schematic of **(c)** band bending by Au and **(d)** plasmon-induced charge separation due to photochemical reactions at the metal/semiconductor heterojunctions. Here, heterocomponents (Ti and Ba) and white contrast due to silver deposition could act as a site for surface reaction. The striped pattern of these deposits is consistent with the domain structure and polarization-specific reactivity flux. The crystallographic orientations of the faces are labeled. **(e)** HRTEM images showing chemically tight heterojunctions between PdO–Co_3O_4 nanoparticles synthesized in the gas phase. Such heterojunction is clearly observed between the single-crystalline PdO particle, oriented in the (002) direction, and a single-crystalline Co_3O_4 particle, oriented in the (111) direction. **(f)** A *p*-type semiconductor (holes are charge carriers) showing charge transfer from Co_3O_4 to PdO via heterojunctions for surface reaction. Adapted with permission from Zhang et al. (2014) and Zhang and Yates (2012). Copyright 2012 and 2014, American Chemical Society.

heteroaggregates provided that the two dissimilar particles have large differences in atomic numbers (high atomic number particles are usually brighter) in HAADF-STEM images (**Fig. 4**).

4. Heteroaggregation, interface properties, and applications

4.1 Band bending at the heteroaggregate interface

Heteroaggregation at the nanoscale (heterojunctions) allows the development of unique functional properties that are essential for many industrial applications. The presence of heterojunctions between two dissimilar particles allows Femi level equilibration and transfer of charge via the space charge layer to the particle with high work function energy. Hence, such tight hetero-contacts are key to these applications, including but not limited to catalysis (hydrocarbon cracking, dry reforming of methane, organic molecular degradation etc.), chemical sensors, electronics, and energy storage technologies (Carlsson et al., 2023; Wang et al., 2021). The number of hetero-contacts in the aggregates depends on the production routes for heteroaggregates, and the degree of mixing is further understood via mathematical modeling of the mixing processes followed by experimental verification of the heteroaggregate formation (Gerken et al., 2023).

The degree of mixing in the gas-phase process depends on the composition, metal components, and their concentration in the solid solution (Liu et al., 2020). Many particles, including but not limited to doping, solid solution, and mixed metal oxide phases, have been produced following this route (Kho et al., 2011; Manshian et al., 2017; Stark et al., 2003; Teoh et al., 2007; Xiao et al., 2011, 2013). The synthesis of particles may be limited by their thermodynamic properties, e.g., differences in vapor pressures, boiling points, and solid–solid miscibility. These are important in high-temperature synthesis where solid-state reactions and/or the formation of complex oxide mixtures are obtained. Although the mixing of heteroatoms is a parameter inclusive of mathematical variance as a measure of inhomogeneity, a description of the functionality of heteroaggregated particle systems is necessary (Grossmann, 2017). The particle–particle and/or hetero-atomic interaction originates through the contact between different particles, through the resulting interface, or via contacts, as depicted in **Fig. 4** (Zhang et al., 2014). Properties such as charge, mass, heat transfer, and even chemical reactions are realized through such hetero-contacts, explaining the involvement of the number of contact regions/interfaces in controlling the material properties of the overall system (Gerken et al., 2023). For instance, charge transfer across

heterojunctions determines the mechanism involved in surface reactions such as chemical sensors, catalysis and biological redox assessment, and nanomedicines (Minnermann et al., 2011; Möller et al., 2013; Naatz et al., 2020; Takenaka et al., 2012; Xiao et al., 2011).

4.2 Charge transfer across the particle–particle heterojunction

Metal–metal oxide heterojunctions are also important because the charges can be transferred through the resulting band bending supporting the $e^{-}h^{+}$ pair separation. The key properties of such catalysts include (1) eluding $e^{-}h^{+}$ pair recombination during the photocatalytic reaction, (2) enhanced reactive sites on the large specific surface, and (3) shifting the optical absorption edge via particle engineering (Yu et al., 2018; Zhang et al., 2012). Zhang et al. (2011) reported the photoreduction of Ag^{+} on $BaTiO_3$ microcrystals physically visualized via white particles in hetero-contact with the (100) and (111) planes [**Figs. 4(a) and (b)**]. The reactivity of the surfaces in the order of (100) > (111) > (110) was related to the heterojunction in the Ag-ferroelectric crystal. The charge transfer and band bending due to the heterojunction at the Au/TiO_2 surface are shown in **Fig. 4(c)**. The presence of downward band bending via electropositive Au on the O_2/TiO_2 (110) heterojunction surface slows down the hole transport via the space charge layer. In both cases, the separated e^{-} and h^{+} participate in the chemical reactions [see **Fig. 4(d)**]. The valence electrons in the metal particle are collectively excited via photon adsorption (surface plasmon resonance). Excited electrons with energy higher than the Schottky barrier cross metal/semiconductor heterojunctions and transfer to the valence band of the semiconductor (Zhang et al., 2011; Zhang and Yates, 2012). In another report, George et al. (2011) reported the photochemical properties of Fe-doped TiO_2 synthesized in the gas phase using flame spray pyrolysis. The increasing dopant (via hetero-contact) in TiO_2 reciprocally decreased the band gap energy of the particles and was able to excite electrons at the absorption edge near visible light (George et al., 2011; Gomes et al., 2023). Such an effect demonstrates the importance of band energy in photocatalysis. Zhang et al. functionalized PdO on Co_3O_4 to create surface PdO/Co_3O_4 heterojunctions (Lin et al., 2011). The Fermi energy alignment between PdO and Co_3O_4 triggered e^{-} transfer from Co_3O_4 to PdO at the interface, resulting in h^{+} generation, as shown in **Figs. 4(e) and (f)**. While surface engineering and modification strategies ease the separation of $e^{-}h^{+}$ pairs on the surface for enhanced photocatalytic efficiency, the significant number density of such charge pairs recombines in the bulk before surface migration for the redox process. The success of the photocatalytic process relies on the effective separation of the photogenerated charges $e^{-}h^{+}$ in the bulk before they take part in the surface redox reaction (George et al., 2011; Lin et al., 2011). The charge transfer concepts described above are also valid in catalysis/photocatalysis and electrochemical processes. Such transfer is particularly attractive when *p*- and *n*-type junctions are realized, for example, in chemical sensors (Frisenda et al., 2018).

4.3 Particle–particle heterojunction in chemical sensors

Jeong et al. reported the formation of Cr_2O_3–SnO_2 sensors for the detection of ethylene at low concentrations. The cross-sectional imaging showed a uniform sensor thickness of ~21 μm [**Fig. 5(a)**]. High-magnification images of the top layer showed spherical SnO_2 covered by Cr_2O_3 nanoparticles, resulting in a rough surface shown in **Figs. 5(b) and (c)**. The layer composition of the sensor had a uniform distribution of the metals and oxygen, as depicted in **Figs. 5(d) and (e)**, while the Cr distribution was on top of the Sn layer with a heterojunction. The cross-responses of the Cr_2O_3–SnO_2 to amines such as dimethylene and/or trimethylamine and NH_3 (meat or fish usually emit these amines when stored) is a unique sensing marker. The sensing data showed that the specific distances between the fruit and the sensing system successfully discriminated bananas for different levels of ripening. The ethylene recognition test for a banana in the absence and presence of seafood and/or meat using $0.3Cr_2O_3$–SnO_2 sensor showed that the ethylene response was unaffected during storage. In addition, Cr_2O_3–SnO_2 bilayer sensor potentially monitored in real-time and onsite fruit freshness via a portable sensing device was connected to a mobile phone via WLAN, as shown in **Figs. 5(f) and (g)**. A strategy for detecting ethylene at a low ppm concentration shows the importance of heterojunction for efficient gas sensing. The analyte gas adsorption behavior and/or surface reactions are quite different for various molecules on solid surfaces. For instance, a surface with sufficient adsorption energy might support molecular cleavage and allow intermediate species to diffuse to the neighboring particle for further reaction via hetero-contact (Jeong et al., 2020). The SnO_2–Cr_2O_3 heterojunction was highly selective and sensitive toward ethylene due to the catalytic oxidation of reactive interfering gases, without sacrificing the transport of the analyte gas to the lower sensing region across the heterojunction.

The sintering of the powder sample is another process that intensifies the particle–particle heterojunction via heat treatment. During exothermic surface reactions, heat transport occurs from one component to the other and propagates to neighboring surfaces through hetero-contacts. For example, heat transfer in gas sensors provides suitable adsorption and reaction conditions, leading to improved sensitivity (Gardner et al., 2023). Naik et al. reported the gas sensing properties of WO_3–ZnO system and showed that the sintering of grains seemed easier in composites rich in

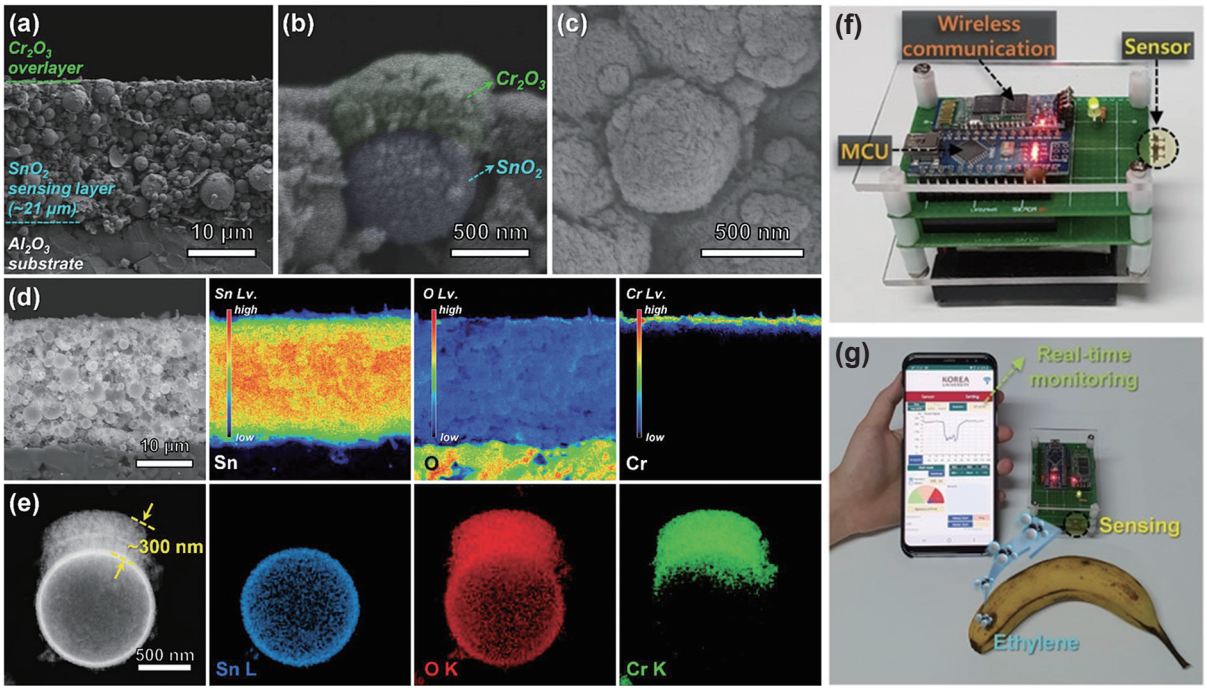

Fig. 5 Imaging and hetero-contact characterization of Cr_2O_3-SnO_2 based sensor detecting ethylene (C_2H_4) gas: **(a)** cross-sectional image of the heterostructured film, **(b)** magnified SEM image clearly showing Cr_2O_3-SnO_2 heterojunction, **(c)** top-view image, **(d)** elemental mapping images of Sn, O, and Cr mapping, **(e)** elemental mapping images of Sn, O, and Cr with color codes showing detachment of a particle from the top region of the sensing film, **(f)** wireless sensor module used to assess and monitor fruit freshness using Cr_2O_3-SnO_2 sensing film, **(g)** photograph of the in situ gas-sensing test. Adapted with permission from a reference (Jeong et al., 2020). Copyright 2020, WILEY-VCH Verlag.

either WO_3 or ZnO. The extent of hetero-contacts was higher in the mixture with low and high amounts of oxides, e.g., 10%ZnO and 90%WO_3, rather than 50%WO_3 and 50%ZnO where inhomogeneity in the mixing was observed. This observation is in line with the highest sensing response by 10%ZnO–90%WO_3 for NO_2 at an operating temperature of 300 °C (Naik et al., 2013). In another report, Shimizu et al. (2001) significantly increased the NO response of 5.0 wt.% Cr_2O_3–SnO_2 hetero-contacts via the formation of *p*–*n* junctions. Tuning particle–particle heterojunction allows direct adjustment of the accumulation or depletion layer, surface catalytic activity, Lewis–Bronsted acid–base properties, and polarity, which are key to catalytic application (Jo et al., 2022).

4.4 Heteroaggregation and its application in catalysis

While the gas sensing property of heteroaggregates depends on the mixing and increased number of hetero-contacts, such particle geometry is also important for catalytic reactions. As stated in **Section 2**, heteroaggregates can be tailor-made using a double flame system, and the particles are controlled via homogeneous mixing of the aerosol streams (Gockeln et al., 2018b; Kemmler et al., 2012; Manshian et al., 2018; Naatz et al., 2017, 2020; Pokhrel and Mädler, 2020). To realize catalytic performance based on mixing and/or with an increased number of hetero-contacts [see **Fig. 6 (upper panel)**], a series of Pt–Ba/Al_2O_3 and Pt/Ba/$Ce_xZr_{1-x}O_2$ multicomponent catalysts with various Ba loadings (4.5–33 wt%) were prepared using a double flame unit and tested for NOx storage capacity (Strobel et al., 2006). The in situ HT-$BaCO_3$ phase leads to improved NO*x* storage potential at higher Ba loadings (Piacentini et al., 2006). In another report, the hetero-contacts between catalytically active Co and Al_2O_3 support and their defined particle size were controlled using different intersection distances of the particle streams in the two independent nozzles. The catalytic material was stable on the Al_2O_3 support during FT synthesis with enhanced performance (Minnermann et al., 2013). Høj et al. (2013) used multiple flame systems to prepare a heterogeneous catalyst including (CoMo) in Al_2O_3 support. The hydrodenitrogenation activity of the catalysts without heat treatment improved from 71 % to 91 % after mixing two aerosol streams. The chemoselective hydrogenation of aromatic ketones was performed using double flame-generated Pd/silica–alumina catalysts. The Pd particles offered identical electronic properties on the Pd surface, contributing similar chemoselectivity for the hydrogenation of carbonyl groups on all double-flame-derived catalysts. Hydrogenation was strongly enhanced by tuning the density of the surface Brønsted acid sites on the catalytic support by varying the Si/Al hetero-contact density (Wang et al., 2013). Very recently, Gäßler et al. (2022) reported the methylation activity of catalysts, namely Co/SiO_2, Co/TiO_2, and Co/TiO_2–SiO_2. The synthesis technique and in situ mixing

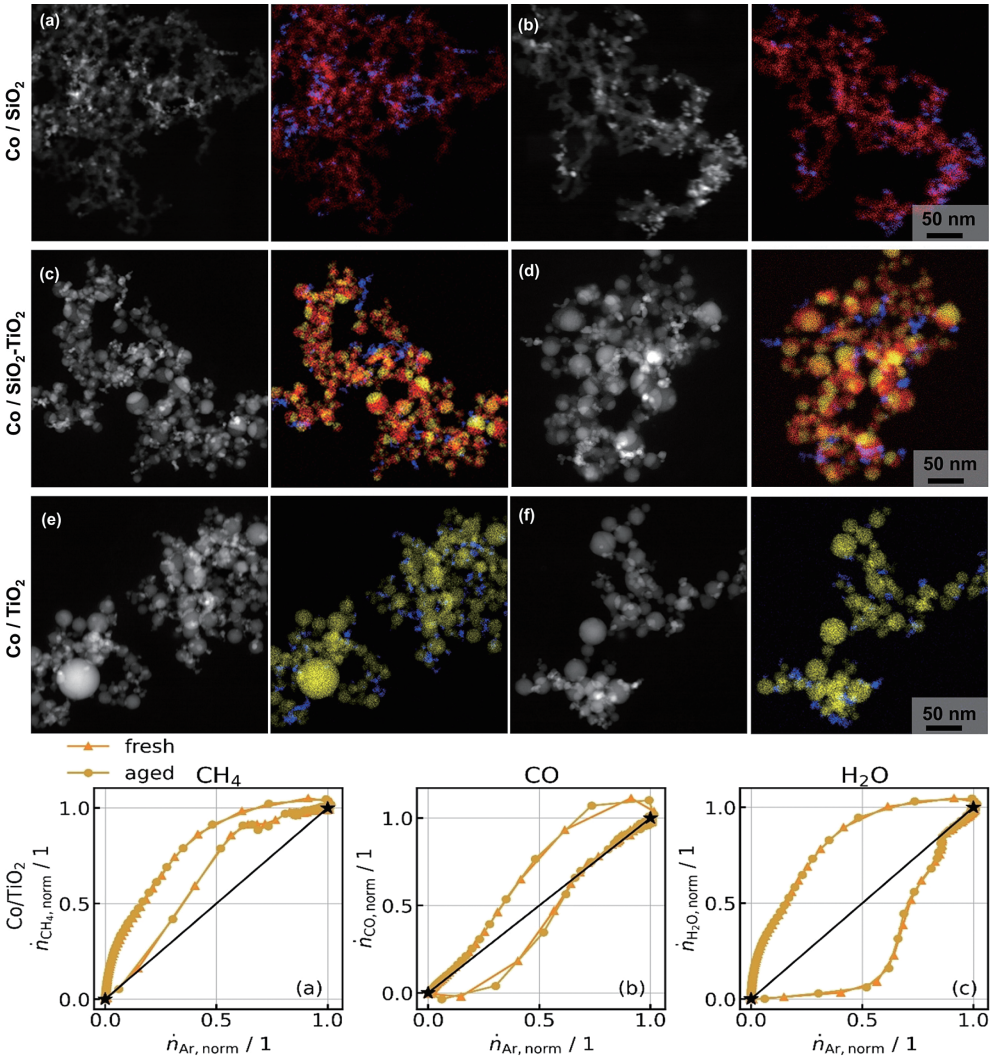

Fig. 6 **(upper panel)** TEM micrographs of Co/SiO_2 **(a,b)**, Co/SiO_2-TiO_2 **(c,d)**, and Co/TiO_2 **(e,f)** catalysts. The micrographs in HAADF mode and EDX mappings of the elements show Co in blue, Si in red, and Ti in yellow. **(lower panel)** State-space plots for outlet molar flow rates of CH_4, CO, and H_2O for Co/TiO_2 catalysts at 300 °C and 2 bar. Adapted from Gäßler et al. (2022). Copyright 2022 Wiley.

were suitable for well-defined heteroaggregates catalysts. The separation of the individual nanoparticle formation into two independent flames and varying nozzle distances allowed for the defined mixing of active metal and support.

Dynamic catalytic testing showed that the support material is affected by adsorbed H_2O on the support surface, leading to a significant delay in H_2O response. In contrast, the data showed fast formation of stoichiometric CH_4 [**Fig. 6 (lower panel)**]. While the formation of CO is increased with Co/TiO_2–SiO_2, the rate of CH_4 formation increases with higher TiO_2 fractions in the support (Gäßler et al., 2022). In another report, Stahl et al. (2021) studied Co/Al_2O_3, Co/Pt, Co/ZrO_2, and Co/Sm_2O_3 heteroaggregated catalysts synthesized by double-flavor gas phase mixing. The results of different surface promoters, including Pt, ZrO_2 and Sm_2O_3, showed overall improvement of methanation at operation temperature compared with unpromoted catalyst. In the case of CO methanation, Pt performed the best methanation activation, and all the catalysts deactivated rapidly above 310 °C. The combination of well-defined catalysts obtained from the gas phase provides the basis to correlate material properties with catalytic performance (Stahl et al., 2021). In the future, experiments with doping on the reactive surface might even lead to the formation of catalytically very active heteroaggregates. Hence, the particle properties depend on the degree of mixing and are directly proportional to the number of hetero-contacts in the aggregates. Selectivity, which is essential in heterogeneous catalysis, e.g., layered double hydroxide (LDH), allows polymerization of propylene oxide on the hydroxide surface. Laycock et al. (1991) reported that inorganic or organometallic coordination is possible on the specific orientation of the LDH surface for heterojunction.

The optimal functionality of the material also depends on the contact area, atomic structure of the interface, lattice strain, and defect chemistry of the two dissimilar particles. The variation in the process parameters during double

flame spray pyrolysis allows efficient mixing and results in improved functionalities in various other applications.

4.5 Particle–particle heteroaggregation in photocatalysis

The heterojunctions in the aggregates improve the photocatalytic activity by enhancing charge carrier separation and reducing recombination. Selective deposition with active co-catalysts allows enhancement of the number of heterojunctions. Apart from the $e^{-}h^{+}$ pair separation, the extension of light absorption by the combination of at least one visible light-absorbing semiconductor hetero-contact also enhances the catalytic property (Marschall, 2014). The photocatalytic reaction of sucrose with excess oxygen favors a reductive pathway in Pt/TiO_2 heteroaggregates (Teoh et al., 2005). However, the photocatalytic reaction of methanol was absent, clearly indicating the beneficial effects of Pt(0) and/or Pt(IV) hetero-contact with TiO_2 (Teoh et al., 2005; 2007). The photocatalysis using different Pt functionalized hetero-contacts showed an optimum photocatalytic effect for 0.5 % Pt loading. At a lower Pt distribution (0.1 %), the activity was even lower than that of pure TiO_2 due to the high photocurrent density of the Pt particles enhancing the electron–hole recombination process (Teoh et al., 2005). To test this effect, Kho et al. (2010) studied photocatalytic H_2 evolution over aqueous TiO_2 using methanol as a hole scavenger. The variation in the band energies of the anatase and rutile phases poses a synergic barrier and electron transfer across the anatase–rutile junction, as depicted in **Figs. 7(A) and (C)**. Such synergistic behavior (charge separation mechanism in the interface of the heteroaggregates) is responsible for the photoactivity of the particles. The other possibility of $e^{-}h^{+}$ pair generation in the TiO_2 based nanoparticles is via re-engineering oxides by doping (hetero-contacts), as shown in **Figs. 7(B) and (D)**(George et al., 2011). The effect in the mixed anatase–rutile phases originated through efficient charge separation across the interface. In another report, Sasikala et al. (2009) reported TiO_2–SnO_2 heteroaggregates with enhanced photocatalytic activity for hydrogen generation compared with pure TiO_2 via effective charge separation in the aggregate system. Similarly, Jia et al. (2014) studied $BiVO_4$–$SrTiO_3$: Rh heterojunction system and reported that a stable interface between components is essential for charge separation. The heteroaggregation and structural complexity of the photocatalyst components described above offer many

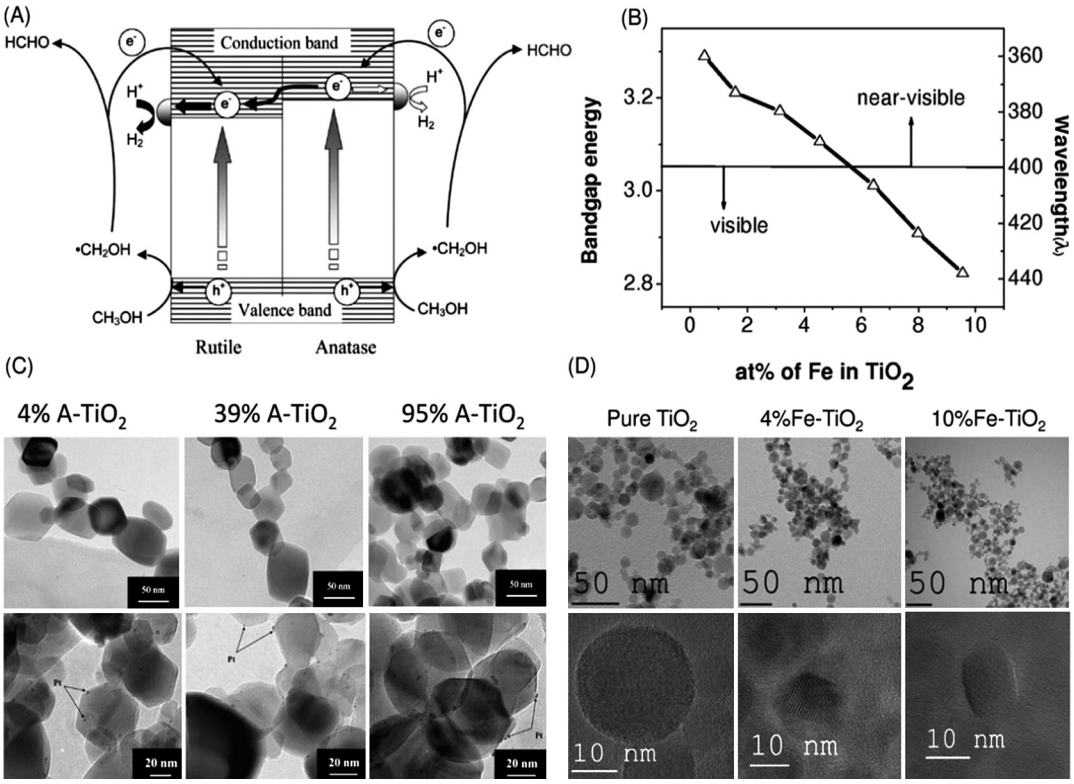

Fig. 7 **(A)** Proposed photocatalytic route for H_2 evolution via electron transfer in the anatase–rutile heterojunction. The oxidation of methanol results in the formation of hydroxymethyl radicals (CH_2OH) via hydroxyl radicals (OH). **(B)** Decrease in the band gap energy by Fe doping in TiO_2. With an increase in the doping content, the band gap energy decreases. **(C)** (**Top**): Images of TiO_2 nanoparticles with 4, 39 and 95 % anatase contents. **Bottom**: Images of Pt/TiO_2 (4, 39 and 95 % anatase) with Pt dispersion after photocatalytic reaction. **(D)** Microscopic images of undoped and Fe-doped TiO_2 nanoparticles. Low-resolution (**top row**) and high-resolution (**bottom row**) images of single particles of undoped TiO_2, 4 % Fe doped TiO_2 and 10 % Fe-doped TiO_2, respectively. Adapted with permission from references (George et al., 2011; Kho et al., 2010). Copyright 2010 and 2011, American Chemical Society.

degrees of freedom for tuning their catalytic properties (Schauermann et al., 2013).

4.6 Heteroaggregation in energy storage applications

Apart from the performance of the catalysis, heteroaggregates with tight chemical contact are also known to be very novel for the development of energy storage materials (designed from the double flame spray pyrolysis). While single-phase $LiMn_2O_4$ has a high energy density and rate capability, the dissolution of Mn^{2+} in the electrolyte via disproportionation causes cell degradation and fast capacity fading (Erichsen et al., 2020). The use of double flame gas phase synthesis, efficient mixing of two aerosol streams inclined at constant 20° (one with $AlPO_4$ and the second with $LiMn_2O_4$), produced $AlPO_4/LiMn_2O_4$ heteroaggregates in the gas phase. The electrochemical performances of these energy storage materials showed a capacity retention of 93 % and an outstanding initial capacity of 116.1 mAh g^{-1} for 1 % $AlPO_4$, as depicted in **Figs. 8(a)–(c)** (Li et al., 2021).

In another report, novel battery systems were fabricated using double flame spray pyrolysis followed by a role-to-role lamination technique. The C–$Li_4Ti_5O_{12}$ heterojunction was obtained by combusting xylene in one independent flame and $Li_4Ti_5O_{12}$ in the other flame , as illustrated in **Figs. 8(d) and (e)**. The carbon stream was mixed with the active energy storage material above the

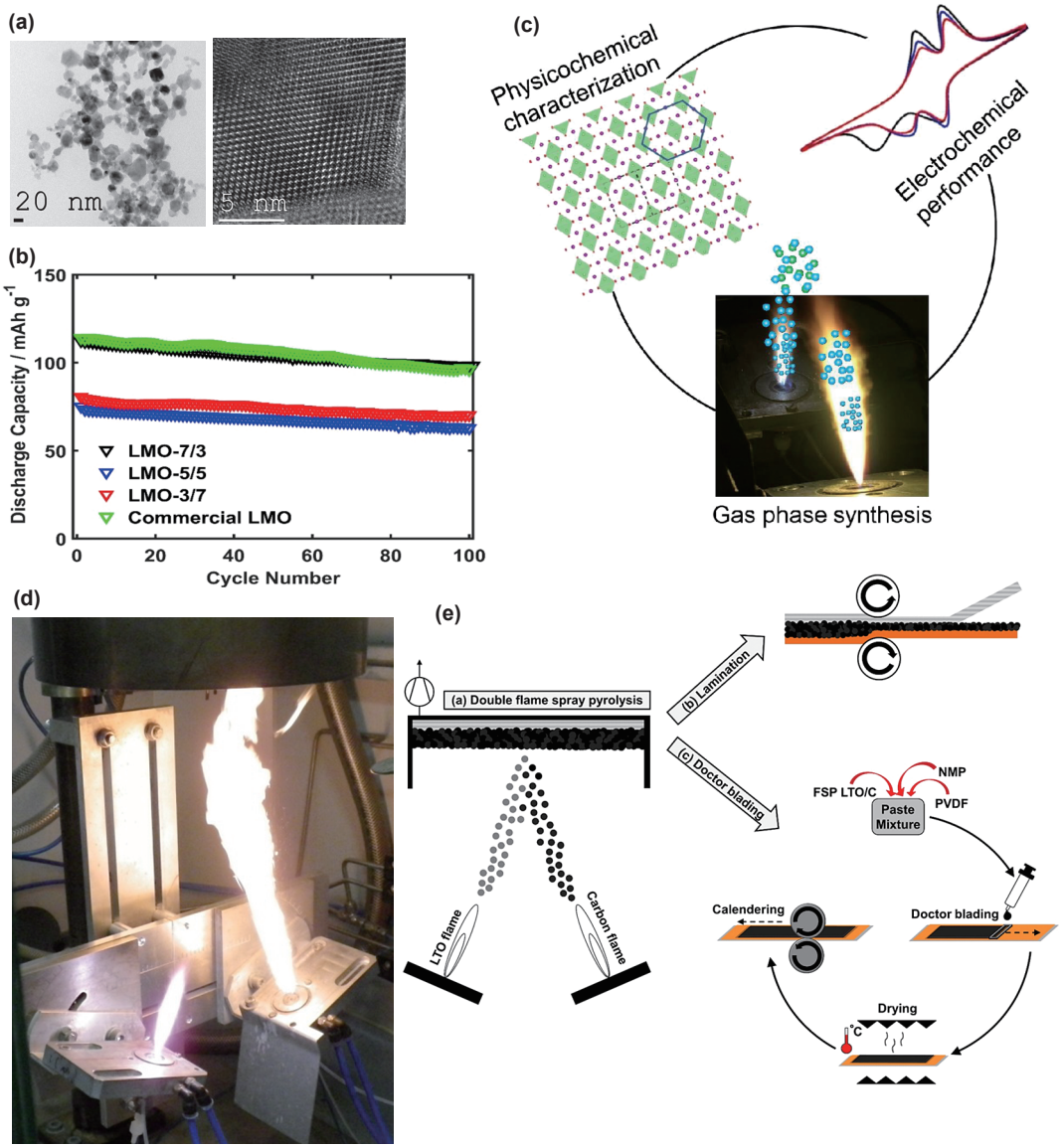

Fig. 8 Energy storage heteroaggregated materials: **(a)–(c)** particle characterization and energy storage application of heteroaggregated $AlPO_4$ with spinel $LiMn_2O_4$. The material is a promising cathode for rechargeable Li-ion batteries because of its cost effectiveness, eco-friendliness, high energy density, and rate capability. **(d)** Synthesis of C–$Li_4Ti_5O_{12}$ using double-flavor aerosol mixing, **(e)** realization of role-to-role layer transfer technology and doctor blading for battery layer fabrication. Adapted from references (Gockeln et al., 2018b; Li et al., 2021). Copyright: 2018 American Chemical Society 2018 and 2021 Elsevier.

flame. The C–$Li_4Ti_5O_{12}$ powder was transferred to the current collector directly from the role-to-role laminator.

The development of this in situ gas-phase process avoids (1) the use of organic binder and/or solvent and (2) the traditional multiple steps necessary for battery fabrication (Ernst et al., 2007; Li et al., 2021). As described above for $AlPO_4$–$LiMn_2O_4$ and C–$Li_4Ti_5O_{12}$ lithium-ion batteries, these batteries have come into industrial focus with high interest. The investment in cathode, anode, and electrolytic research has been realized due to solid–liquid hetero-contact (Groß, 2022). The results showed that the solid electrolytes interfaced with the solid electrodes were free from leakage, free from Li-dendrite growth, and non-flammable during cycling, as depicted in **Figs. 9(a)–(d)**. These advantages allowed feasible battery operation at a wide range of temperatures (Meng et al., 2022). All solid-state batteries covering a large class of materials including but not limited to polymeric, inorganic ceramic, or glassy materials such as oxides, halides, and sulfides with tight hetero-contact are commercially attractive, and a few of them are already under operation and use (Manthiram et al., 2017; Naatz et al., 2018; Pokhrel et al., 2023; Zou et al., 2020).

4.7 Particle–particle heterojunction in superconductors and medicine

The physical properties, including but not limited to charge transfer, specific band energy position changes, spin–orbit, and spin–spin coupling, can be altered by increasing the number of hetero-contacts through doping, pressing, and sintering. Gan et al. (2023) designed an oxide hetero-contact using $Hf_{0.5}Zr_{0.5}O_2$ interfaced with a selective orientation (110) of $KTaO_3$, allowing light-induced giant spin–orbit coupling-based superconducting interfaces. Such hetero-contacts are promising efficient spintronic devices and topological superconductors. While heteroaggregation is a key to many physical properties and applications, such heteroaggregation is equally important in medicinal and pharmaceutical processes for efficient treatment. Meng et al. (2010) used mesoporous SiO_2 nanoparticles as a solid support for controlled drug delivery using their large surface for functionalization (solid–solid hetero-contact) to control the nanopore openings. These particles were used as a novel delivery system based on the function of such hetero-contacts. In recent years, various approaches such as deep-eutectic systems (Sánchez-Leija et al., 2014), solid crystal suspensions, and nanoparticulate formulations (Ely et al., 2014) have been shown to have the best performance due to the interaction effect in the

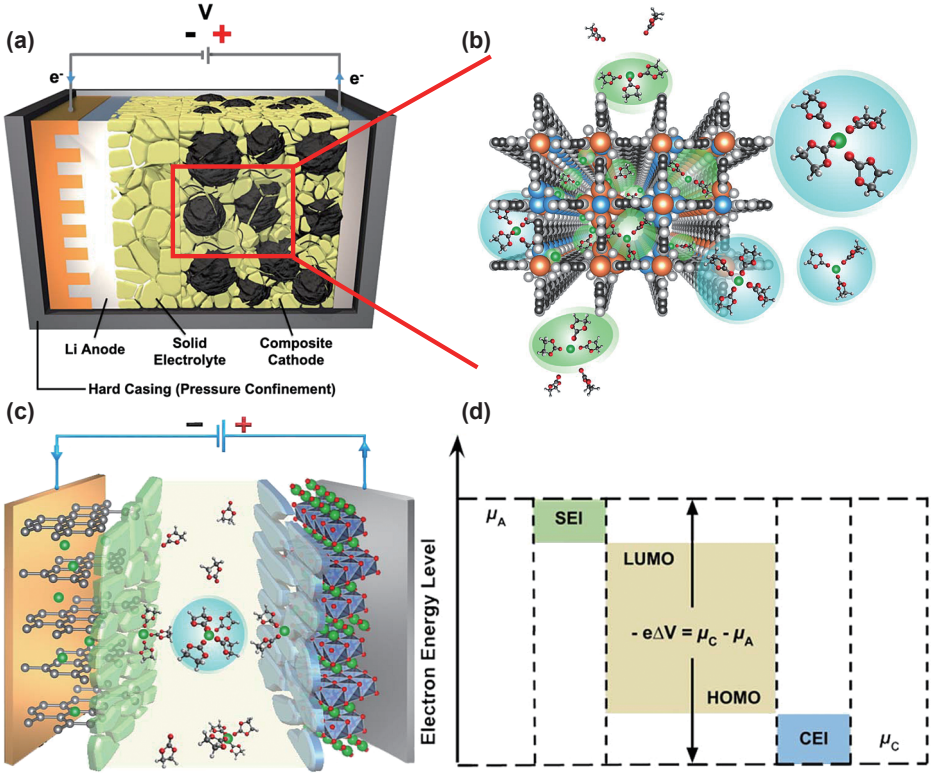

Fig. 9 **(a)** All solid-state lithium ion batteries showing hetero-contacts between the electrodes and electrolyte, **(b)** solvation in nanoconfinement within the cells with hetero-junctions, **(c)** Schematic diagram showing hetero-junctions with all battery components with stable ionic conduction in the electrolyte, **(d)** electrodes operating at potentials beyond the region enclosed between energy levels followed by interphase formation for the reversibility of the cell chemistry. Adapted with permission from a reference (Meng et al., 2022). Copyright 2022, American Association for the Advancement of Science.

colloidal size (Priemel et al., 2012). This effect is achieved by the local hetero-contact of the multicomponent substances at the nanoscale.

4.8 Layer fabrication with heteroaggregates

The transfer of forces and moments at the hetero-contact occurs during the densification and layering of the powders. To design such systems, the combination of ductile and brittle particles offers a high-strength granular system that allows deformations at the interfaces. Baric et al. (2019) modeled nanoparticle aggregate film compaction (considering elastic sinter bridges between primary particles) using DEM. The results showed deviation from the experimentally determined porosity and pore size distribution against applied pressure when non-covalence, adhesion, very rigid, and strong agglomerates were considered [**Figs. 10(a)–(e)**]. Such porosity of the films arises from low mechanical resistance. The thermal stability of the films was realized via sintering/annealing to enhance electrical conductivity; however, this was at the expense of the reduced porosity and specific surface area. In the gas phase, in situ thermophoresis for the development of heterojunctions involves high-velocity particle streams colliding with the substrates placed above the spray. The post treatments,

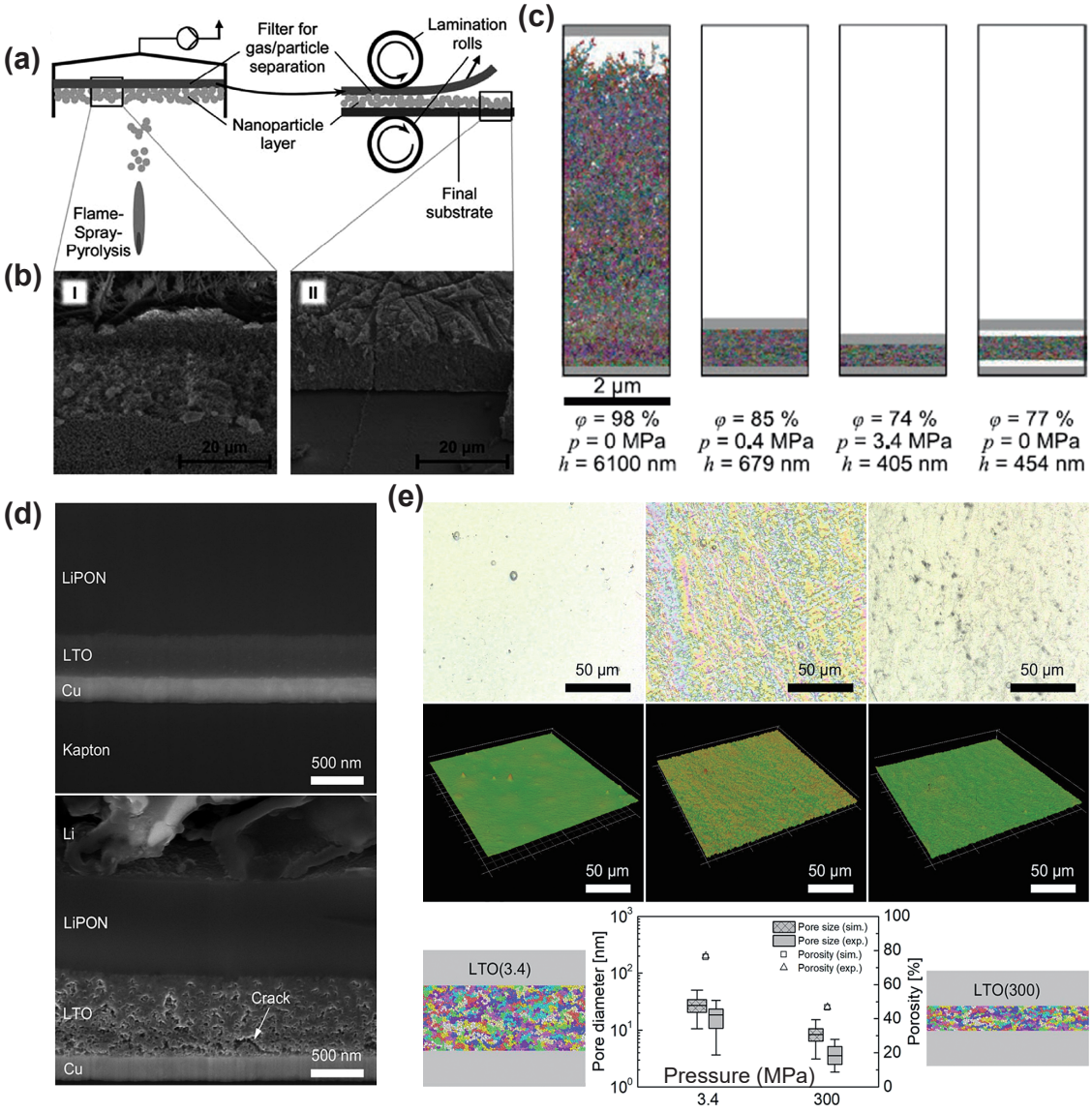

Fig. 10 **(a)–(c)** Role-to-role layer transfer of in situ deposited particles. **(a)** Gas phase synthesis of heteroaggregates and layer transfer via lamination. **(b)** SEM images of the fabricated layer **(I)** before and **(II)** after layer transfer. **(c)** Simulation of the thermophoretic particle layer. The φ, p, and h denote the porosity, pressure, and film height, respectively. **(d)** Thin-film lithium-ion batteries overview and $Li_4Ti_5O_{12}$ close-up images of SEM/FIB cuts for $Li_4Ti_5O_{12}$ at 300 **(top)** and 3.4 **(lower)** MPa pressure. The higher pressured $Li_4Ti_5O_{12}$ at 300 MPa is dense, homogeneous, and thin, whereas the lower pressured layer is porous, irregular, and thicker. **(e)** 2D **(top)** and 3D **(middle)** representations of the surface sections of $Li_4Ti_5O_{12}$ powder, compacted at 0, 3.4, and 300 MPa **(e-lower panel)** illustrate the coherence of the simulated and experimental porosities and pore size distributions of $Li_4Ti_5O_{12}$ at 3.4 and 300 MPa, respectively. The colored images on the left and right in **(e)** demonstrate the simulated thin films. Adapted with permission from references (Gockeln et al., 2020; Pokhrel and Mädler, 2020). Copyright 2020, American Chemical Society.

i.e., sintering the resulting particle–particle heteroaggregates, are unnecessary because organic binders are avoided at all process steps and the temperature of combustion is ~3000 °C. While particle–substrate bonding strength (loose hetero-contact of the layer with the substrate) is weaker for the in situ deposited layers, Schopf et al. (2013) developed a role-to-role lamination process enabling compact dry nanoparticle films at pressures up to 3.4 MPa. Such role-to-role layer fabrication technology allowed stronger and mechanically stable hetero-contact between the substrate and the particle layer, as shown in **Figs. 10(a) and (b)**.

The compaction led to a significant increase in the compressive Young's modulus (from 0.8 MPa to 1.9 MPa) and a decrease in porosity from 84 % to 79 % while preserving the specific surface area of the film, as depicted in **Figs. 10(d) and (e)**. In addition, it has been reported that compact particle–particle films retain their physical properties, e.g., structure and morphology, against capillary forces resulting from an air–liquid interface during liquid imbibition (Schopf et al., 2017). It must be noted that particles of 10 nm size at 3.4 MPa compaction pressure producing brittle fractures is highly unlikely. To validate this finding, flexible $Li_4Ti_5O_{12}$ layers (LTO) were in situ deposited on Cu substrates (LTO–Cu hetero-contact) followed by compacting at pressures of 3.4 and 300 MPa. The hetero-contact at higher pressure was dense, homogeneous, and thin, whereas the contact compacted at lower pressure was highly porous, more irregular, and thicker, as shown in **Figs. 10(d) and (e)**. The LTO–Cu hetero-contact compressed at 300 MPa and 3.4 MPa showed porosities of 46.6 % and 76.7 %, matching the DEM-simulated porosities of 46.4 % and 75.9 %, respectively (Gockeln et al., 2018a; 2018b; 2020). Gottschalk et al. (2023) reported high-energy hetero-contacts of C–Si. The data showed that the balanced ratio of the active heteroaggregates and compaction drives the battery performance optimally.

5. Conclusion and outlook

The development of process parameters to design a large number of particle–particle hetero-contacts during production is a key to many innovative applications. The generation of hetero-contacts within the heteroaggregates allows specific charge distributions in the particle–particle interface, providing a great opportunity to develop new materials in the gas phase. However, unresolved challenges such as but not limited to surface adsorption, particle shape/size, and turbulence in the gas phase affect the actual realization of particle mixing. While larger process time length, particle concentrations, and homogeneity gradients of the mixing are particularly challenging, the quantification of such heteroaggregates and the determination of parameters for such aggregation create new opportunities and resolve the drawbacks, i.e., heteromixing, which is difficult via liquid phase and/or physical mixing processes. The non-uniform heteroaggregation is caused by different mixing zones during the spray, while the mixing of two aerosol streams crossing at an angle differs significantly in the flow direction. Two identical free jets at different distances from each other result in very different mixing patterns in the flow direction. This makes it possible to mix particles that meet at very different growth stages, control over heteroaggregation. This review aims to establish functional correlationsbetween the process design, modeling, particle–particle mixing, and uniformity of the heteroaggregates. These aggregates at the nanoscale are a very important class of materials, especially in catalysis, sensor, and battery development. Charge transport between different components and different heterojunctions is the driving factor for enhanced performance. The same applies to semiconducting materials, where the *n*–*p* transition within heteroaggregates is another emerging field of research. On this basis, new concepts for gas sensors and photoreactors have been developed. In addition, in catalysis, mass and charge transfers in multicomponent materials are important. Hence, to realize an advancement in science, especially in materials science, particle formulation and the characterization of heteroaggregates are research topics with high relevance.

Acknowledgments

The authors thank the German Research Foundation (DFG) for funding through the priority program SPP 2289 Hetero-Aggregates. SP and LM would like to thank the European Research Council (ERC) for Grant Agreement 786487.

References

Adeleye A.S., Pokhrel S., Mädler L., Keller A.A., Influence of nanoparticle doping on the colloidal stability and toxicity of copper oxide nanoparticles in synthetic and natural waters, Water Research, 132 (2018) 12–22. https://doi.org/10.1016/j.watres.2017.12.069

Balakrishnan A., Groeneveld J.D., Pokhrel S., Mädler L., Metal sulfide nanoparticles: precursor chemistry, Chemistry – A European Journal, 27 (2021) 6390–6406. https://doi.org/10.1002/chem.202004952

Baric V., Ciacchi L.C., Mädler L., Compaction-induced restructuring of aggregated nanoparticle films using the discrete element method, Powder Technology, 342 (2019) 773–779. https://doi.org/10.1016/j.powtec.2018.10.038

Baric V., Grossmann H.K., Koch W., Mädler L., Quantitative characterization of mixing in multicomponent nanoparticle aggregates, Particle & Particle Systems Characterization, 35 (2018) 1800177. https://doi.org/10.1002/ppsc.201800177

Buss L., Meierhofer F., Bianchi Neto P., França Meier H., Fritsching U., Noriler D., Impact of co-flow on the spray flame behaviour applied to nanoparticle synthesis, The Canadian Journal of Chemical Engineering, 97 (2019) 604–615. https://doi.org/10.1002/cjce.23386

Carlsson A., Rosen J., Dahlqvist M., Finding stable multi-component materials by combining cluster expansion and crystal structure predictions, npj Computational Materials, 9 (2023) 21. https://doi.org/10.1038/s41524-023-00971-3

Dreyer J.A.H., Pokhrel S., Birkenstock J., Hevia M.G., Schowalter M., Rosenauer A., Urakawa A., Teoh W.Y., Mädler L., Decrease of the required dopant concentration for δ-Bi_2O_3 crystal stabilization through thermal quenching during single-step flame spray pyrolysis,

CrystEngComm, 18 (2016) 2046–2056. https://doi.org/10.1039/c5ce02430g

Eggersdorfer M.L., Kadau D., Herrmann H.J., Pratsinis S.E., Aggregate morphology evolution by sintering: number and diameter of primary particles, Journal of Aerosol Science, 46 (2012) 7–19. https://doi.org/10.1016/j.jaerosci.2011.11.005

Ely D.R., Edwin García R., Thommes M., Ostwald–Freundlich diffusion-limited dissolution kinetics of nanoparticles, Powder Technology, 257 (2014) 120–123. https://doi.org/10.1016/j.powtec.2014.01.095

Endres S.C., Avila M., Mädler L., A discrete differential geometric formulation of multiphase surface interfaces for scalable multiphysics equilibrium simulations, Chemical Engineering Science, 257 (2022) 117681. https://doi.org/10.1016/j.ces.2022.117681

Endres S.C., Ciacchi L.C., Mädler L., A review of contact force models between nanoparticles in agglomerates, aggregates, and films, Journal of Aerosol Science, 153 (2021) 105719. https://doi.org/10.1016/j.jaerosci.2020.105719

Erichsen T., Pfeiffer B., Roddatis V., Volkert C.A., Tracking the diffusion-controlled lithiation reaction of $LiMn_2O_4$ by in situ TEM, ACS Applied Energy Materials, 3 (2020) 5405–5414. https://doi.org/10.1021/acsaem.0c00380

Ernst F.O., Kammler H.K., Roessler A., Pratsinis S.E., Stark W.J., Ufheil J., Novák P., Electrochemically active flame-made nanosized spinels: $LiMn_2O_4$, $Li_4Ti_5O_{12}$ and $LiFe_5O_8$, Materials Chemistry and Physics, 101 (2007) 372–378. https://doi.org/10.1016/j.matchemphys.2006.06.014

Feng J., Biskos G., Schmidt-Ott A., Toward industrial scale synthesis of ultrapure singlet nanoparticles with controllable sizes in a continuous gas-phase process, Scientific Reports, 5 (2015) 15788. https://doi.org/10.1038/srep15788

Feng J., Huang L., Ludvigsson L., Messing M.E., Maisser A., Biskos G., Schmidt-Ott A., General approach to the evolution of singlet nanoparticles from a rapidly quenched point source, The Journal of Physical Chemistry C, 120 (2016) 621–630. https://doi.org/10.1021/acs.jpcc.5b06503

Fischer D., Börzsönyi T., Nasato D.S., Pöschel T., Stannarius R., Heaping and secondary flows in sheared granular materials, New Journal of Physics, 18 (2016) 113006. https://doi.org/10.1088/1367-2630/18/11/113006

Frisenda R., Molina-Mendoza A.J., Mueller T., Castellanos-Gomez A., van der Zant H.S.J., Atomically thin p–n junctions based on two-dimensional materials, Chemical Society Reviews, 47 (2018) 3339–3358. https://doi.org/10.1039/c7cs00880e

Gan Y., Yang F., Kong L., Chen X., Xu H., Zhao J., Li G., Zhao Y., Yan L., Zhong Z., Chen Y., Ding H., Light-induced giant Rashba spin–orbit coupling at superconducting $KTaO_3$(110) heterointerfaces, Advanced Materials, 35 (2023) 2300582. https://doi.org/10.1002/adma.202300582

Gardner E.L.W., Gardner J.W., Udrea F., Micromachined thermal gas sensors—a review, Sensors, 23 (2023) 681. https://doi.org/10.3390/s23020681

Gäßler M., Stahl J., Schowalter M., Pokhrel S., Rosenauer A., Mädler L., Güttel R., The impact of support material of cobalt-based catalysts prepared by double flame spray pyrolysis on CO_2 methanation dynamics, ChemCatChem, 14 (2022) e202200286. https://doi.org/10.1002/cctc.202200286

George S., Pokhrel S., Ji Z., Henderson B.L., Xia T., Li L., Zink J.I., Nel A.E., Mädler L., Role of Fe doping in tuning the band gap of TiO_2 for the photo-oxidation-induced cytotoxicity paradigm, Journal of the American Chemical Society, 133 (2011) 11270–11278. https://doi.org/10.1021/ja202836s

Gerken B., Mahr C., Stahl J., Grieb T., Schowalter M., Krause F.F., Mehrtens T., Mädler L., Rosenauer A., Material discrimination in nanoparticle hetero-aggregates by analysis of scanning transmission electron microscopy images, Particle & Particle Systems Characterization, 40 (2023) 2300048. https://doi.org/10.1002/ppsc.202300048

Gockeln M., Glenneberg J., Busse M., Pokhrel S., Mädler L., Kun R., Flame aerosol deposited $Li_4Ti_5O_{12}$ layers for flexible, thin film all-solid-state Li-ion batteries, Nano Energy, 49 (2018a) 564–573. https://doi.org/10.1016/j.nanoen.2018.05.007

Gockeln M., Pokhrel S., Meierhofer F., Glenneberg J., Schowalter M., Rosenauer A., Fritsching U., Busse M., Mädler L., Kun R., Fabrication and performance of $Li_4Ti_5O_{12}$/C Li-ion battery electrodes using combined double flame spray pyrolysis and pressure-based lamination technique, Journal of Power Sources, 374 (2018b) 97–106. https://doi.org/10.1016/j.jpowsour.2017.11.016

Gockeln M., Ruiter T., Palacios Saura A., Baric V., Glenneberg J., Busse M., Pokhrel S., Kun R., Mädler L., Enhancing the utilization of porous $Li_4Ti_5O_{12}$ layers for thin-film lithium-ion batteries, ACS Applied Energy Materials, 3 (2020) 9667–9675. https://doi.org/10.1021/acsaem.0c01231

Gomes S.I.L., Roca C.P., Pokhrel S., Mädler L., Scott-Fordsmand J.J., Amorim M.J.B., TiO_2 nanoparticles' library toxicity (UV and non-UV exposure) – high-throughput in vivo transcriptomics reveals mechanisms, NanoImpact, 30 (2023) 100458. https://doi.org/10.1016/j.impact.2023.100458

Gottschalk L., Oertel C., Strzelczyk N., Müller J., Krüger J., Haselrieder W., Kwade A., Improving the performance of lithium-ion batteries using a two-layer, hard carbon-containing silicon anode for use in high-energy electrodes, Energy Technology, 11 (2023) 2200858. https://doi.org/10.1002/ente.202200858

Groß A., Reversible vs standard hydrogen electrode scale in interfacial electrochemistry from a theoretician's atomistic point of view, The Journal of Physical Chemistry C, 126 (2022) 11439–11446. https://doi.org/10.1021/acs.jpcc.2c02734

Grossmann H.K., Tailored aerosol synthesis of nanosized multicomponent catalysts, PhD, University of Bremen, 2017, <https://media.suub.uni-bremen.de/handle/elib/1464> accessed 29122023.

Grossmann H.K., Grieb T., Meierhofer F., Hodapp M.J., Noriler D., Gröhn A., Meier H.F., Fritsching U., Wegner K., Mädler L., Nanoscale mixing during double-flame spray synthesis of heterostructured nanoparticles, Journal of Nanoparticle Research, 17 (2015) 174. https://doi.org/10.1007/s11051-015-2975-8

Gröhn A.J., Buesser B., Jokiniemi J.K., Pratsinis S.E., Design of turbulent flame aerosol reactors by mixing-limited fluid dynamics, Industrial & Engineering Chemistry Research, 50 (2011) 3159–3168. https://doi.org/10.1021/ie1017817

Gunkelmann N., Montaine M., Pöschel T., Stochastic behavior of the coefficient of normal restitution, Physical Review E, 89 (2014) 022205. https://doi.org/10.1103/physreve.89.022205

Høj M., Pham D., Brorson M., Mädler L., Jensen A., Grunwaldt J.-D., Two-nozzle flame spray pyrolysis (FSP) synthesis of CoMo/Al_2O_3 hydrotreating catalysts, Catalysis Letters, 143 (2013) 386–394. https://doi.org/10.1007/s10562-013-0990-x

Horlyck J., Pokhrel S., Lovell E., Bedford N.M., Mädler L., Amal R., Scott J., Unifying double flame spray pyrolysis with lanthanum doping to restrict cobalt–aluminate formation in Co/Al_2O_3 catalysts for the dry reforming of methane, Catalysis Science & Technology, 9 (2019) 4970–4980. https://doi.org/10.1039/c9cy01293a

Jeong S.-Y., Moon Y.K., Kim T.-H., Park S.-W., Kim K.B., Kang Y.C., Lee J.-H., A new strategy for detecting plant hormone ethylene using oxide semiconductor chemiresistors: exceptional gas selectivity and response tailored by nanoscale Cr_2O_3 catalytic overlayer, Advanced Science, 7 (2020) 1903093. https://doi.org/10.1002/advs.201903093

Jia Q., Iwase A., Kudo A., $BiVO_4$–Ru/$SrTiO_3$:Rh composite Z-scheme photocatalyst for solar water splitting, Chemical Science, 5 (2014) 1513–1519. https://doi.org/10.1039/c3sc52810c

Jo Y.-M., Jo Y.K., Lee J.-H., Jang H.W., Hwang I.-S., Yoo D.J., MOF-based chemiresistive gas sensors: toward new functionalities, Advanced Materials, 35 (2022) 2206842. https://doi.org/10.1002/adma.202206842

Johannessen T., Pratsinis S.E., Livbjerg H., Computational fluid-particle dynamics for the flame synthesis of alumina particles, Chemical Engineering Science, 55 (2000) 177–191. https://doi.org/10.1016/S0009-2509(99)00183-9

Kemmler J.A., Pokhrel S., Birkenstock J., Schowalter M., Rosenauer A., Bârsan N., Weimar U., Mädler L., Quenched, nanocrystalline $In_4Sn_3O_{12}$ high temperature phase for gas sensing applications, Sensors and Actuators B: Chemical, 161 (2012) 740–747.

https://doi.org/10.1016/j.snb.2011.11.026
Kho Y.K., Iwase A., Teoh W.Y., Mädler L., Kudo A., Amal R., Photocatalytic H_2 evolution over TiO_2 nanoparticles. The synergistic effect of anatase and rutile, The Journal of Physical Chemistry C, 114 (2010) 2821–2829. https://doi.org/10.1021/jp910810r
Kho Y.K., Teoh W.Y., Iwase A., Mädler L., Kudo A., Amal R., Flame preparation of visible-light-responsive $BiVO_4$ oxygen evolution photocatalysts with subsequent activation via aqueous route, ACS Applied Materials & Interfaces, 3 (2011) 1997–2004. https://doi.org/10.1021/am200247y
Kim K.D., Pokhrel S., Wang Z., Ling H., Zhou C., Liu Z., Hunger M., Mädler L., Huang J., Tailoring high-performance Pd catalysts for chemoselective hydrogenation reactions via optimizing the parameters of the double-flame spray pyrolysis, ACS Catalysis, 6 (2016) 2372–2381. https://doi.org/10.1021/acscatal.6b00396
Kruis F.E., Kusters K.A., Pratsinis S.E., Scarlett B., A simple model for the evolution of the characteristics of aggregate particles undergoing coagulation and sintering, Aerosol Science and Technology, 19 (1993) 514–526. https://doi.org/10.1080/02786829308959656
Laycock D.E., Collacott R.J., Alan Skelton D., Tchir M.F., Stereospecific polymerization of propylene oxide on thermally activated synthetic hydrotalcite, Journal of Catalysis, 130 (1991) 354–358. https://doi.org/10.1016/0021-9517(91)90119-o
Li H., Erinmwingbovo C., Birkenstock J., Schowalter M., Rosenauer A., La Mantia F., Mädler L., Pokhrel S., Double flame-fabricated high-performance $AlPO_4$/$LiMn_2O_4$ cathode material for Li-Ion batteries, ACS Applied Energy Materials, 4 (2021) 4428–4443. https://doi.org/10.1021/acsaem.1c00024
Li H., Pokhrel S., Schowalter M., Rosenauer A., Kiefer J., Mädler L., The gas-phase formation of tin dioxide nanoparticles in single droplet combustion and flame spray pyrolysis, Combustion and Flame, 215 (2020) 389–400. https://doi.org/10.1016/j.combustflame.2020.02.004
Lin S., Zhao Y., Xia T., Meng H., Ji Z., Liu R., George S., Xiong S., Wang X., Zhang H., Pokhrel S., Mädler L., Damoiseaux R., Lin S., Nel A.E., High content screening in zebrafish speeds up hazard ranking of transition metal oxide nanoparticles, ACS Nano, 5 (2011) 7284–7295. https://doi.org/10.1021/nn202116p
Liu C., Pokhrel S., Tessarek C., Li H., Schowalter M., Rosenauer A., Eickhoff M., Li S., Mädler L., Rare-earth-doped $Y_4Al_2O_9$ nanoparticles for stable light-converting phosphors, ACS Applied Nano Materials, 3 (2020) 699–710. https://doi.org/10.1021/acsanm.9b02231
Lovell E.C., Großman H., Horlyck J., Scott J., Mädler L., Amal R., Asymmetrical double flame spray pyrolysis-designed SiO_2/$Ce_{0.7}Zr_{0.3}O_2$ for the dry reforming of methane, ACS Applied Materials & Interfaces, 11 (2019) 25766–25777. https://doi.org/10.1021/acsami.9b02572
Mädler L., Kammler H.K., Mueller R., Pratsinis S.E., Controlled synthesis of nanostructured particles by flame spray pyrolysis, Journal of Aerosol Science, 33 (2002) 369–389. https://doi.org/10.1016/s0021-8502(01)00159-8
Manshian B.B., Pokhrel S., Himmelreich U., Tämm K., Sikk L., Fernández A., Rallo R., Tamm T., Mädler L., Soenen S.J., In silico design of optimal dissolution kinetics of Fe-doped ZnO nanoparticles results in cancer-specific toxicity in a preclinical rodent model, Advanced Healthcare Materials, 6 (2017) 1601379. https://doi.org/10.1002/adhm.201601379
Manshian B.B., Pokhrel S., Mädler L., Soenen S.J., The impact of nanoparticle-driven lysosomal alkalinization on cellular functionality, Journal of Nanobiotechnology, 16 (2018) 85. https://doi.org/10.1186/s12951-018-0413-7
Manthiram A., Yu X., Wang S., Lithium battery chemistries enabled by solid-state electrolytes, Nature Reviews Materials, 2 (2017) 16103. https://doi.org/10.1038/natrevmats.2016.103
Marine W., Patrone L., Luk'yanchuk B., Sentis M., Strategy of nanocluster and nanostructure synthesis by conventional pulsed laser ablation, Applied Surface Science, 154–155 (2000) 345–352. https://doi.org/10.1016/s0169-4332(99)00450-x
Marschall R., Semiconductor composites: strategies for enhancing charge carrier separation to improve photocatalytic activity, Advanced Functional Materials, 24 (2014) 2421–2440. https://doi.org/10.1002/adfm.201303214
Meierhofer F., Fritsching U., Synthesis of metal oxide nanoparticles in flame sprays: review on process technology, modeling, and diagnostics, Energy & Fuels, 35 (2021) 5495–5537. https://doi.org/10.1021/acs.energyfuels.0c04054
Meierhofer F., Hodapp M., Achelis L., Buss L., Noriler D., Meier H.F., Fritsching U., Investigation of atomization concepts for large-scale flame spray pyrolysis (FSP), Materialwissenschaft und Werkstofftechnik, 45 (2014) 765–778. https://doi.org/10.1002/mawe.201400314
Meierhofer F., Li H., Gockeln M., Kun R., Grieb T., Rosenauer A., Fritsching U., Kiefer J., Birkenstock J., Mädler L., Pokhrel S., Screening precursor–solvent combinations for $Li_4Ti_5O_{12}$ energy storage material using flame spray pyrolysis, ACS Applied Materials & Interfaces, 9 (2017) 37760–37777. https://doi.org/10.1021/acsami.7b11435
Meng H., Xue M., Xia T., Zhao Y.-L., Tamanoi F., Stoddart J.F., Zink J.I., Nel A.E., Autonomous in vitro anticancer drug release from mesoporous silica nanoparticles by pH-sensitive nanovalves, Journal of the American Chemical Society, 132 (2010) 12690–12697. https://doi.org/10.1021/ja104501a
Meng Y.S., Srinivasan V., Xu K., Designing better electrolytes, Science, 378 (2022) eabq3750. https://doi.org/10.1126/science.abq3750
Minnermann M., Grossmann H.K., Pokhrel S., Thiel K., Hagelin-Weaver H., Bäumer M., Mädler L., Double flame spray pyrolysis as a novel technique to synthesize alumina-supported cobalt Fischer–Tropsch catalysts, Catalysis Today, 214 (2013) 90–99. https://doi.org/10.1016/j.cattod.2013.04.001
Minnermann M., Pokhrel S., Thiel K., Henkel R., Birkenstock J., Laurus T., Zargham A., Flege J.-I., Zielasek V., Piskorska-Hommel E., Falta J., Mädler L., Bäumer M., Role of palladium in iron based Fischer–Tropsch catalysts prepared by flame spray pyrolysis, The Journal of Physical Chemistry C, 115 (2011) 1302–1310. https://doi.org/10.1021/jp106860d
Möller W., Gibson N., Geiser M., Pokhrel S., Wenk A., Takenaka S., Schmid O., Bulgheroni A., Simonelli F., Kozempel J., Holzwarth U., Wigge C., Eigeldinger-Berthou S., Mädler L., Kreyling W.G., Gold nanoparticle aerosols for rodent inhalation and translocation studies, Journal of Nanoparticle Research, 15 (2013) 1574. https://doi.org/10.1007/s11051-013-1574-9
Munnik P., de Jongh P.E., de Jong K.P., Recent developments in the synthesis of supported catalysts, Chemical Reviews, 115 (2015) 6687–6718. https://doi.org/10.1021/cr500486u
Naatz H., Hoffmann R., Hartwig A., La Mantia F., Pokhrel S., Mädler L., Determination of the flat band potential of nanoparticles in porous electrodes by blocking the substrate–electrolyte contact, The Journal of Physical Chemistry C, 122 (2018) 2796–2805. https://doi.org/10.1021/acs.jpcc.7b11423
Naatz H., Lin S., Li R., Jiang W., Ji Z., Chang C.H., Köser J., Thöming J., Xia T., Nel A.E., Mädler L., Pokhrel S., Safe-by-design CuO nanoparticles via Fe-doping, Cu–O bond length variation, and biological assessment in cells and zebrafish embryos, ACS Nano, 11 (2017) 501–515. https://doi.org/10.1021/acsnano.6b06495
Naatz H., Manshian B.B., Rios Luci C., Tsikourkitoudi V., Deligiannakis Y., Birkenstock J., Pokhrel S., Mädler L., Soenen S.J., Model-based nanoengineered pharmacokinetics of iron-doped copper oxide for nanomedical applications, Angewandte Chemie International Edition, 59 (2020) 1828–1836. https://doi.org/10.1002/anie.201912312
Naik A.J.T., Parkin I.P., Binions R., Gas sensing studies of an n-n heterojunction metal oxide semiconductor sensor array based on WO_3 and ZnO composites, Sensors, 2013 IEEE, (2013) 1–4. https://doi.org/10.1109/icsens.2013.6688509
Noriler D., Rosebrock C.D., Madler L., Meier H.F., Fritsching U., Influence of atomization and spray parameters on the flame spray process for nanoparticle production, 24 (2014) 495–524. https://doi.org/10.1615/AtomizSpr.2014008559
Parteli E.J.R., Pöschel T., Particle-based simulation of powder application in additive manufacturing, Powder Technology, 288 (2016) 96–102.

https://doi.org/10.1016/j.powtec.2015.10.035
Parteli E.J.R., Schmidt J., Blümel C., Wirth K.-E., Peukert W., Pöschel T., Attractive particle interaction forces and packing density of fine glass powders, Scientific Reports, 4 (2014) 6227. https://doi.org/10.1038/srep06227
Pfeiffer T.V., Feng J., Schmidt-Ott A., New developments in spark production of nanoparticles, Advanced Powder Technology, 25 (2014) 56–70. https://doi.org/10.1016/j.apt.2013.12.005
Piacentini M., Strobel R., Maciejewski M., Pratsinis S.E., Baiker A., Flame-made Pt–Ba/Al_2O_3 catalysts: structural properties and behavior in lean-NO_x storage-reduction, Journal of Catalysis, 243 (2006) 43–56. https://doi.org/10.1016/j.jcat.2006.07.005
Pokhrel S., Birkenstock J., Schowalter M., Rosenauer A., Mädler L., Growth of ultrafine single crystalline WO_3 nanoparticles using flame spray pyrolysis, Crystal Growth & Design, 10 (2010) 632–639. https://doi.org/10.1021/cg9010423
Pokhrel S., Mädler L., Flame-made particles for sensors, catalysis, and energy storage applications, Energy & Fuels, 34 (2020) 13209–13224. https://doi.org/10.1021/acs.energyfuels.0c02220
Pokhrel S., Nel A.E., Mädler L., Custom-designed nanomaterial libraries for testing metal oxide toxicity, Accounts of Chemical Research, 46 (2013) 632–641. https://doi.org/10.1021/ar300032q
Pokhrel S., Stahl J., Groeneveld J.D., Schowalter M., Rosenauer A., Birkenstock J., Mädler L., Flame aerosol synthesis of metal sulfides at high temperature in oxygen-lean atmosphere, Advanced Materials, 35 (2023) 2211104. https://doi.org/10.1002/adma.202211104
Pöschel T., Schwager T., Computational Granular Dynamics-Models and Algorithms, Springer, Berlin, Heidelberg, New York, 2005, ISBN: 978-3540214854. https://doi.org/10.1007/3-540-27720-x
Pratsinis S.E., Flame aerosol synthesis of ceramic powders, Progress in Energy and Combustion Science, 24 (1998) 197–219. https://doi.org/10.1016/s0360-1285(97)00028-2
Priemel P.A., Grohganz H., Gordon K.C., Rades T., Strachan C.J., The impact of surface- and nano-crystallisation on the detected amorphous content and the dissolution behaviour of amorphous indomethacin, European Journal of Pharmaceutics and Biopharmaceutics, 82 (2012) 187–193. https://doi.org/10.1016/j.ejpb.2012.05.012
Sánchez-Leija R.J., Pojman J.A., Luna-Bárcenas G., Mota-Morales J.D., Controlled release of lidocaine hydrochloride from polymerized drug-based deep-eutectic solvents, Journal of Materials Chemistry B, 2 (2014) 7495–7501. https://doi.org/10.1039/c4tb01407c
Sasikala R., Shirole A., Sudarsan V., Sakuntala T., Sudakar C., Naik R., Bharadwaj S.R., Highly dispersed phase of SnO_2 on TiO_2 nanoparticles synthesized by polyol-mediated route: photocatalytic activity for hydrogen generation, International Journal of Hydrogen Energy, 34 (2009) 3621–3630. https://doi.org/10.1016/j.ijhydene.2009.02.085
Schauermann S., Nilius N., Shaikhutdinov S., Freund H.-J., Nanoparticles for heterogeneous catalysis: new mechanistic insights, Accounts of Chemical Research, 46 (2013) 1673–1681. https://doi.org/10.1021/ar300225s
Schopf S.O., Hartwig A., Fritsching U., Mädler L., Imbibition into highly porous layers of aggregated particles, Transport in Porous Media, 119 (2017) 119–141. https://doi.org/10.1007/s11242-017-0876-2
Schopf S.O., Salameh S., Mädler L., Transfer of highly porous nanoparticle layers to various substrates through mechanical compression, Nanoscale, 5 (2013) 3764–3772. https://doi.org/10.1039/c3nr34235b
Schubert M., Pokhrel S., Thomé A., Zielasek V., Gesing T.M., Roessner F., Mädler L., Bäumer M., Highly active Co–Al_2O_3-based catalysts for CO_2 methanation with very low platinum promotion prepared by double flame spray pyrolysis, Catalysis Science & Technology, 6 (2016) 7449–7460. https://doi.org/10.1039/c6cy01252c
Shi S., Russell T.P., Nanoparticle assembly at liquid–liquid interfaces: from the nanoscale to mesoscale, Advanced Materials, 30 (2018) 1800714. https://doi.org/10.1002/adma.201800714
Shimizu Y., Nakashima N., Hyodo T., Egashira M., NO_x sensing properties of varistor-type gas sensors consisting of micro p-n junctions, Journal of Electroceramics, 6 (2001) 209–217. https://doi.org/10.1023/A:1011448513611
Stahl J., Ilsemann J., Pokhrel S., Schowalter M., Tessarek C., Rosenauer A., Eickhoff M., Bäumer M., Mädler L., Comparing co-catalytic effects of ZrO_x, SmO_x, and Pt on CO_x methanation over Co-based catalysts prepared by double flame spray pyrolysis, ChemCatChem, 13 (2021) 2815–2831. https://doi.org/10.1002/cctc.202001998
Stark W.J., Maciejewski M., Mädler L., Pratsinis S.E., Baiker A., Flame-made nanocrystalline ceria/zirconia: structural properties and dynamic oxygen exchange capacity, Journal of Catalysis, 220 (2003) 35–43. https://doi.org/10.1016/S0021-9517(03)00235-5
Strobel R., Mädler L., Piacentini M., Maciejewski M., Baiker A., Pratsinis S.E., Two-nozzle flame synthesis of Pt/Ba/Al_2O_3 for NO_x storage, Chemistry of Materials, 18 (2006) 2532–2537. https://doi.org/10.1021/cm0600529
Sun B., Pokhrel S., Dunphy D.R., Zhang H., Ji Z., Wang X., Wang M., Liao Y.-P., Chang C.H., Dong J., Li R., Mädler L., Brinker C.J., Nel A.E., Xia T., Reduction of acute inflammatory effects of fumed silica nanoparticles in the lung by adjusting silanol display through calcination and metal doping, ACS Nano, 9 (2015) 9357–9372. https://doi.org/10.1021/acsnano.5b03443
Sun B., Wang X., Liao Y.-P., Ji Z., Chang C.H., Pokhrel S., Ku J., Liu X., Wang M., Dunphy D.R., Li R., Meng H., Mädler L., Brinker C.J., Nel A.E., et al., Repetitive dosing of fumed silica leads to profibrogenic effects through unique structure–activity relationships and biopersistence in the lung, ACS Nano, 10 (2016) 8054–8066. https://doi.org/10.1021/acsnano.6b04143
Tabrizi N.S., Xu Q., van der Pers N.M., Lafont U., Schmidt-Ott A., Synthesis of mixed metallic nanoparticles by spark discharge, Journal of Nanoparticle Research, 11 (2009) 1209–1218. https://doi.org/10.1007/s11051-008-9568-8
Takenaka S., Möller W., Semmler-Behnke M., Karg E., Wenk A., Schmid O., Stoeger T., Jennen L., Aichler M., Walch A., Pokhrel S., Mädler L., Eickelberg O., Kreyling W.G., Efficient internalization and intracellular translocation of inhaled gold nanoparticles in rat alveolar macrophages, Nanomedicine, 7 (2012) 855–865. https://doi.org/10.2217/nnm.11.152
Teoh W.Y., Denny F., Amal R., Friedmann D., Mädler L., Pratsinis S.E., Photocatalytic mineralisation of organic compounds: a comparison of flame-made TiO_2 catalysts, Topics in Catalysis, 44 (2007) 489–497. https://doi.org/10.1007/s11244-006-0096-4
Teoh W.Y., Mädler L., Beydoun D., Pratsinis S.E., Amal R., Direct (one-step) synthesis of TiO_2 and Pt/TiO_2 nanoparticles for photocatalytic mineralisation of sucrose, Chemical Engineering Science, 60 (2005) 5852–5861. https://doi.org/10.1016/j.ces.2005.05.037
Topic N., Pöschel T., Steepest descent ballistic deposition of complex shaped particles, Journal of Computational Physics, 308 (2016) 421–437. https://doi.org/10.1016/j.jcp.2015.12.052
Ulrich G.D., Subramanian N.S., III. Coalescence as a rate-controlling process, Combustion Science and Technology, 17 (1977) 119–126. https://doi.org/10.1080/00102207708946822
Voloshko A., Colombier J.-P., Itina T.E., Comparison of laser ablation with spark discharge techniques used for nanoparticle production, Applied Surface Science, 336 (2015) 143–149. https://doi.org/10.1016/j.apsusc.2014.10.077
Wang F., Harindintwali J.D., Yuan Z., Wang M., Wang F., Li S., Yin Z., Huang L., Fu Y., Li L., Chang S.X., Zhang L., Rinklebe J., Yuan Z., Zhu Q., et al., Technologies and perspectives for achieving carbon neutrality, The Innovation, 2 (2021) 100180. https://doi.org/10.1016/j.xinn.2021.100180
Wang H., Adeleye A.S., Huang Y., Li F., Keller A.A., Heteroaggregation of nanoparticles with biocolloids and geocolloids, Advances in Colloid and Interface Science, 226 (2015) 24–36. https://doi.org/10.1016/j.cis.2015.07.002
Wang Z., Pokhrel S., Chen M., Hunger M., Mädler L., Huang J., Palladium-doped silica–alumina catalysts obtained from double-flame FSP for chemoselective hydrogenation of the model aromatic ketone acetophenone, Journal of Catalysis, 302 (2013) 10–19. https://doi.org/10.1016/j.jcat.2013.02.017
Wu W., Chen K., Tsotsas E., Prediction of particle mixing time in a rotary drum by 2D DEM simulations and cross-correlation, Advanced Powder Technology, 33 (2022) 103512. https://doi.org/10.1016/j.apt.2022.103512
Xiao J., Kuc A., Pokhrel S., Mädler L., Pöttgen R., Winter F., Frauenheim

T., Heine T., Fe-doped ZnO nanoparticles: the oxidation number and local charge on iron, studied by ^{57}Fe Mößbauer Spectroscopy and DFT calculations, Chemistry – A European Journal, 19 (2013) 3287–3291. https://doi.org/10.1002/chem.201204308

Xiao J., Kuc A., Pokhrel S., Schowalter M., Parlapalli S., Rosenauer A., Frauenheim T., Mädler L., Pettersson L.G.M., Heine T., Evidence for Fe^{2+} in wurtzite coordination: iron doping stabilizes ZnO nanoparticles, Small, 7 (2011) 2879–2886. https://doi.org/10.1002/smll.201100963

Yu J., Sun X., Tong X., Zhang J., Li J., Li S., Liu Y., Tsubaki N., Abe T., Sun J., Ultra-high thermal stability of sputtering reconstructed Cu-based catalysts, Nature Communications, 12 (2021) 7209. https://doi.org/10.1038/s41467-021-27557-1

Yu Z., Chen X.-Q., Kang X., Xie Y., Zhu H., Wang S., Ullah S., Ma H., Wang L., Liu G., Ma X., Cheng H.-M., Noninvasively modifying band structures of wide-Bandgap metal oxides to boost photocatalytic activity, Advanced Materials, 30 (2018) 1706259. https://doi.org/10.1002/adma.201706259

Zhang H., Ji Z., Xia T., Meng H., Low-Kam C., Liu R., Pokhrel S., Lin S., Wang X., Liao Y.-P., Wang M., Li L., Rallo R., Damoiseaux R., Telesca D., et al., Use of metal oxide nanoparticle band gap to develop a predictive paradigm for oxidative stress and acute pulmonary inflammation, ACS Nano, 6 (2012) 4349–4368. https://doi.org/10.1021/nn3010087

Zhang H., Pokhrel S., Ji Z., Meng H., Wang X., Lin S., Chang C.H., Li L., Li R., Sun B., Wang M., Liao Y.-P., Liu R., Xia T., Mädler L., et al., PdO doping tunes band-gap energy levels as well as oxidative stress responses to a Co_3O_4 *p*-type semiconductor in cells and the lung, Journal of the American Chemical Society, 136 (2014) 6406–6420. https://doi.org/10.1021/ja501699e

Zhang Z., Tang W., Neurock M., Yates J.T., Jr., Electric charge of single Au atoms adsorbed on TiO_2(110) and associated band bending, The Journal of Physical Chemistry C, 115 (2011) 23848–23853. https://doi.org/10.1021/jp2067809

Zhang Z., Yates J.T., Jr., Band bending in semiconductors: chemical and physical consequences at surfaces and interfaces, Chemical Reviews, 112 (2012) 5520–5551. https://doi.org/10.1021/cr3000626

Zou Z., Li Y., Lu Z., Wang D., Cui Y., Guo B., Li Y., Liang X., Feng J., Li H., Nan C.-W., Armand M., Chen L., Xu K., Shi S., Mobile ions in composite solids, Chemical Reviews, 120 (2020) 4169–4221. https://doi.org/10.1021/acs.chemrev.9b00760

Authors' Short Biographies

Dr. Suman Pokhrel is a "Privatdozent" at the Department of Production Engineering, University of Bremen. His research interests include designing oxide/sulfide nanostructured materials using flame spray pyrolysis (FSP) for various physicochemical applications. His innovative re-engineering of nanoparticles has created cutting-edge research within the nanotechnology field worldwide. Dr. Pokhrel was awarded the Jawaharlal Nehru prize in 2000, the George Forster award of the Alexander von Humboldt foundation in 2006, the JSPS award in 2008, and the Habilitation (Venia Legendi) award in 2016 by the Department of Production Engineering, University of Bremen, for his outstanding contribution in research and teaching.

Prof. Lutz Mädler is a Professor in the Department of Production Engineering and Director of the Leibniz Institute for Materials Science, University of Bremen, Germany. His research includes particle synthesis in the gas phase, catalytic properties, and bio-nano-interactions and has significant contributions in many academic and industrial laboratories worldwide. Prof. Mädler has been the recipient of many awards such as the BASF Award 2004 in Process Engineering, the SMOLUCHOWSKI Award 2005, the DECHEMA Award 2009 (highest award in Chemical Engineering in Germany), and the Leibniz Award 2017. Prof. Mädler is a member of the German Academy of Science and Engineering (acatech).

Prof. Udo Fritsching leads the research group "Multiphase Flow, Heat and Mass Transfer" at the Leibniz Institute for Materials Science, Bremen, Germany, and is a Professor in the Department of Production Engineering at the University of Bremen, Germany. His research interests include multiphase flow, particle technology, atomization, and sprays as well as computational multiphase fluid dynamics and particle and process measurement techniques. Prof. Fritsching serves as the president of ILASS Europe (Institute of Liquid Atomization and Spray Systems) and the chairman of the Multiphase Flow group within VDI/Dechema. He is also a delegate to the Multiphase Flow Working Party of EFCE (European Federation Chemical Engineering).